the reaction mixture, and the resulting solution was stirred at room temperature for 50 h. The aqueous reaction mixture was extracted with Et_2O (30 mL × 3), and the organic extracts were combined, dried over $MgSO_4$, and evaporated to give a residue, which was chromatographed on silica gel (30 g, hexane:acetone = 3:1) to give **13d** (475 mg, 60% in 3 steps) as a pale yellow oil.

4.2. In vitro preferential cytotoxicity

4.2.1. Cells and culture

Human pancreatic cancer cell lines, PANC-1 and CAPAN-1, were maintained in Dulbecco's modified Eagle's medium (DMEM, Nissui Pharmaceutical Co., Ltd., Tokyo, Japan) supplemented with 10% fetal bovine serum (FBS, Gibco BRL Products, Gaithersburg, MD, USA), 0.1% sodium bicarbonate (Nacalai Tesque Inc.), and 1% antibiotic-antimycotic solution (Sigma–Aldrich Inc., St. Louis, MO, USA). Nutrient deprived medium (NDM) contained 265 mg/L $CaCl_2 \cdot 2H_2O$, 0.1 mg/L $Fe(NO_3) \cdot 9H_2O$, 400 mg/L KCl, 200 mg/L $MgSO_4 \cdot 7H_2O$, 6400 mg/L NaCl, 700 mg/L $NaHCO_3$, 125 mg/L NaH_2PO_4, 15 mg/L phenol red, 1 M HEPES buffer (pH 7.4, Wako Pure Chemical Industries, Ltd., Osaka, Japan), and 10 mL MEM vitamin solution (Life Technologies, Inc., Rockville, MD, USA). The final pH was adjusted to 7.4 with 10% $NaHCO_3$. For amino acid supplementation, stock solutions (200 mmol/L L-glutamine solution, MEM amino acids solution, and MEM nonessential amino acids solution; Life Technologies) were added at a concentration of 1%.

4.2.2. Preferential cytotoxicity

Preferential cytotoxicity was determined as previously described [9]. In brief, PANC-1 or CAPAN-1 cells (2×10^4 cells/well) were seeded in 96-well plates (Corning Inc., Corning, NY, USA) and incubated in fresh DMEM at 37 °C under 5% CO_2 and 95% air for 24 h. The cells were washed with Dulbecco's phosphate-buffered saline (PBS, Nissui Pharmaceutical Co., Ltd., Tokyo, Japan) before the medium was replaced with either DMEM or NDM (for CAPAN-1, amino acids-supplimented NDM) containing serial dilutions of the test samples. After 24 h of incubation, the cells were washed with PBS, and 100 μL of DMEM containing 10% WST-8 cell counting kit solution (Dojindo, Kumamoto, Japan) was added to the wells. After 3 h of incubation, the absorbance was measured at 450 nm. Cell viability was calculated from the mean values for three wells using the following equation:

$$\text{Cell viability (\%)} = [(\text{Abs(test samples)} - \text{Abs(blank)})/(\text{Abs((control)} - \text{Abs(blank)})] \times 100$$

The preferential cytotoxicity was expressed as the concentration at which 50% of cells died preferentially in NDM (PC_{50}).

4.3. In vivo antitumor activity of triethoxy derivative 4m in nude mice

Five-week-old female BALB/cAJcl-*nu/nu* mice were obtained from CLEA Japan, Inc. (Tokyo, Japan), and 5×10^6 CAPAN-1 cells in 0.3 mL DMEM were s.c. injected into the right side of the back of the animals. Two weeks later, 12 mice bearing tumors around 5 mm in diameter were randomly divided into treatment groups and a vehicle control group. Because (−)-arctigenin (1) and triethoxy derivative **4m** are poorly soluble in water, they were first dissolved in DMSO at 10 mg/mL and kept frozen until use. Just before administration, the stock solution was diluted in saline to a final concentration of 250 μg/mL (the final concentration of DMSO in saline is 2.5%). The mice were administered by *i.p.*-injections of 0.2 mL of solution of arctigenin, triethoxy derivative **4m**, or vehicle on 6 days of the week for 4 weeks. The tumor size and body weight were measured weekly and the tumor volume was calculated using the following formula: Tumor volume = $4/3 \times 3.14 \times (L/2 \times W/2 \times W/2)$ where L is the length of the tumor and W is its width. Results are expressed as means ±SD. Statistical comparisons were conducted using Student's t test after ANOVA. The results were considered to be significant when $P < 0.05$.

Acknowledgments

This work was supported in part by grants from the Ministry of Health and Welfare for the Third-Term Comprehensive 10-Year Strategy for Cancer Control and by Grant-in-Aid for Scientific Research (C) (No. 22590098) from Japan Society for the Promotion of Science (JSPS).

Appendix A. Supplementary data

Supplementary data related to this article can be found at http://dx.doi:10.1016/j.ejmech.2012.11.031H.

References

[1] J. Ferlay, H.R. Shin, F. Bray, D. Forman, C. Mathers, D.M. Parkin, GLOBOCAN 2008 v1.2, Cancer Incidence and Mortality Worldwide: IARC CancerBase No. 10 (Internet), International Agency for Research on Cancer, Lyon, France, 2010, Available from:, http://globocan.iarc.fr (accessed 08.05.12).
[2] D. Li, K. Xie, R. Wolff, J.L. Abbruzzese, Pancreatic cancer, Lancet 363 (2004) 1049–1057.
[3] S. Shore, D. Vimalachandran, M.G.T. Raraty, P. Ghaneh, Cancer in the elderly: pancreatic cancer, Surg. Oncol. 13 (2004) 201–210.
[4] H.W. Chung, S.M. Bang, S.W. Park, J.B. Chung, J.K. Kang, J.W. Kim, J.S. Seong, W.J. Lee, S.Y. Song, A prospective randomized study of gemcitabine with doxifluridine versus pacritaxel with doxifluridine in concurrent chemo-radiotherapy for locally advanced pancreatic cancer, Int. J. Radiat. Oncol. 60 (2004) 1494–1501.
[5] C.V. Dang, G.L. Semenza, Oncogenic alteration of metabolism, Trends Biochem. Sci. 24 (1999) 68–72.
[6] M. Kitano, M. Kudo, K. Maekawa, Y. Suetomi, H. Sakamoto, N. Fukuta, R. Nakaoka, T. Kawasaki, Dynamic imaging of pancreatic diseases by contrast enhanced coded phase inversion harmonic ultrasonography, Gut 53 (2004) 854–859.
[7] K. Izuishi, K. Kato, T. Ogura, T. Kinoshita, H. Esumi, Remarkable tolerance of tumor cells to nutrient deprivation: possible new biochemical target for cancer therapy, Cancer Res. 60 (2000) 6201–6207.
[8] (a) H. Esumi, J. Lu, Y. Kurashima, T. Hanaoka, Antitumor activity of pyrvinium pamoate, 6-(dimethylamino)-2-[2-(2,5-dimethyl-1-phenyl-1*H*-pyrrol-3-yl) ethenyl]-1-methyl-quinolinium pamoate salt, showing preferential cytotoxicity during glucose starvation, Cancer Sci. 95 (2004) 685–690;
(b) J. Lu, S. Kunimoto, Y. Yamazaki, M. Kaminishi, H. Esumi, D. Kigamicin, A novel anticancer agent based on a new anti-austerity strategy targeting cancer cells' tolerance to nutrient starvation, Cancer Sci. 95 (2004) 547–552.
[9] S. Awale, J. Lu, S.K. Kalauni, Y. Kurashima, Y. Tezuka, S. Kadota, H. Esumi, Identification of arctigenin as an antitumor agent having the ability to eliminate the tolerance of cancer cells to nutrient starvation, Cancer Res. 66 (2006) 1751–1757.
[10] (a) B. Hausott, H. Greger, B. Marian, Naturally occurring lignans efficiently induce apoptosis in colorectal tumor cells, J. Cancer Res. Clin. Oncol. 129 (2003) 569–576;
(b) T. Matsumoto, K. Hosono-Nishiyama, H. Yamada, Antiproliferative and apoptotic effects of butyrolactone lignans from *Arctium lappa* on leukemic cells, Planta Med. 72 (2006) 276–278;
(c) T. Toyoda, T. Tsukamoto, T. Mizoshita, S. Nishibe, T. Deyama, Y. Takenaka, N. Hirano, H. Tanaka, S. Takasu, H. Ban, T. Kumagai, K. Inada, H. Utsunomiya, M. Tatematsu, Inhibitory effect of nordihydroguaiaretic acid, a plant lignan, on *Helicobacter pylori*-associated gastric carcinogenesis in Mongolian gerbils, Cancer Sci. 98 (2007) 1689–1695.
[11] (a) M. Nose, T. Fujimoto, T. Takeda, S. Nishibe, Y. Ogihara, Structural transformation of lignan compounds in rat gastrointestinal tract, Planta Med. 58 (1992) 520–523;
(b) S. Heinonen, T. Nurmi, K. Liukkonen, K. Poutanen, K. Wähälä, T. Deyama, S. Nishibe, H. Adlercreuta, In vitro metabolism of plant lignans: new precursors of mammalian lignans enterolactone and enterodiol, J. Agr. Food Chem. 49 (2001) 3178–3186;
(c) L.-H. Xie, E.-M. Ahn, T. Akao, A.A. Abdel-Hafez, N. Nakamura, M. Hattori, Transformation of arctiin to estrogenic and antiestrogenic substances by human intestinal bacteria, Chem. Pharm. Bull. 51 (2003) 378–384.
[12] E. Eich, H. Pertz, M. Kaloga, J. Schulz, M.R. Fesen, A. Mazumder, Y. Pommier, (−)-Arctigenin as a lead stracture for inhibitors of human immunodeficiency virus type-1 integrase, J. Med. Chem. 39 (1996) 86–95.
[13] M.G. Banwell, S. Chand, G.P. Savage, An enantioselective total synthesis of the stilbenolignan (−)-aiphanol and the determination of its absolute stereochemistry, Tetrahedron: Asymmetry 16 (2005) 1645–1654.

[14] R. Fumeaux, C. Menozzi-Smarrito, A. Stalmach, C. Munari, K. Kraehenbuehl, H. Steiling, A. Crozier, G. Williamson, D. Barron, First synthesis, characterization, and evidence for the presence of hydroxycinnamic acid sulfate and glucuronide conjugates in human biological fluids as a result of coffee consumption, Org. Biomol. Chem. 8 (2010) 5199–5211.

[15] T. Cardinaels, J. Ramaekers, P. Nockemann, K. Driesen, K. Van Hecke, L. Van Meervelt, S. Lei, S. De Feyter, D. Guillon, B. Donnio, K. Binnemans, Imidazo[4,5-f]-1,10-phenanthrolines: versatile ligands for the design of metallomesogens, Chem. Mater. 20 (2008) 1278–1291.

[16] T.C. Daniels, R.E. Lyons, Ethyl esters of triiodophenoxyacetic acids and potassium triiodophenoxyacetate, J. Am. Chem. Soc. 58 (1936) 2646.

[17] M. Lieber, J. Mazzetta, W. Nelson-Rees, M. Kaplan, G. Todaro, Establishment of a continuous tumor-cell line (PANC-1) from a human carcinoma of the exocrine pancreas, Int. J. Cancer 15 (1975) 741–747.

[18] (a) H. Suemizu, M. Monnai, Y. Ohnishi, M. Ito, N. Tamaoki, M. Nakamura, Identification of a key molecular regulator of liver metastasis in human pancreatic carcinoma using a novel quantitative model of metastasis in NOD/SCID/γ_c^{null} (NOG) mice, Int. J. Oncol. 31 (2007) 741–751;
(b) A.P. Kyriazis, A.A. Kyriazis, D.G. Scarpelli, J. Fogh, M.S. Rao, R. Lepera, Human pancreatic adenocarcinoma line Capan-1 in tissue culture and the nude mouse. Morphologic, biologic, and biochemical characteristics, Am. J. Pathol. 106 (1982) 250–260.

[19] S. Koul, B. Singh, S.C. Taneja, G.N. Qazi, New chemo and chemo-enzymatic synthesis of β-benzyl-γ-butyrolactones, Tetrahedron 59 (2003) 3487–3491.

[20] A. Van Oeveren, J.F.G.A. Jansen, B.L. Feringa, Enantioselective synthesis of natural dibenzylbutyrolactone lignans (−)-enterolactone, (−)-hinokinin, (−)-pluviatolide, (−)-enterodiol, and furofuran lignan (−)-eudesmin via tandem conjugate addition tp g-alkoxybutenolides, J. Org. Chem. 59 (1994) 5999–6007.

[21] Aurora Building Blocks, Order Number: A00. 384. 218.

[22] B. Pelcman, J.G.K. Yee, L.F. Macenzie, Y. Zhou, K. Han, Isochromenones as PDE4 and PDE7 inhibitors and their preparation and use in the treatment of inflammation, PCT Int. Appl., 2010076564, 2010.

[23] (a) A. Enoki, M.H. Gold, Degradation of the diarylpropane lignin model compound 1-(3′,4′-diethoxyphenyl)-l,3-dihydroxy-2-(4‴-methoxyphenyl)-propane and derivatives by the basidiomycete *Phanerochaete chrysosporium*, Arch. Microbiol. 132 (1982) 123–130;
(b) V.C. Farmer, M.E.K. Henderson, J.D. Russel, Reduction of certain aromatic acids to aldehydes and alcohols by *Polystictus versicolor*, Biochim. Biophys. Acta 35 (1959) 202–211.

[24] J.A. Dale, S.H. Mosher, Nuclear magnetic resonance enantiomer regents. Configurational correlations via nuclear magnetic resonance chemical shifts of diastereomeric mandelate, O-methylmandelate, and α-methoxy-α-trifluoromethylphenylacetate (MTPA) esters, J. Am. Chem. Soc. 95 (1973) 512–519.

PLOS | ONE

Critical Role of H_2O_2 Generated by NOX4 during Cellular Response under Glucose Deprivation

Satoshi Owada[1,2], Yuko Shimoda[1,2], Katsuya Tsuchihara[1,2], Hiroyasu Esumi[1,2]*

1 Department of Integrated Biosciences, Graduate School of Frontier Sciences, The University of Tokyo, Kashiwa, Japan, **2** Cancer Physiology Project, Research Center for Innovative Oncology, National Cancer Center Hospital East, Kashiwa, Japan

Abstract

Glucose is the most efficient energy source, and various cancer cells depend on glycolysis for energy production. For maintenance of survival and proliferation, glucose sensing and adaptation to poor nutritional circumstances must be well organized in cancer cells. While the glucose sensing machinery has been well studied in yeasts, the molecular mechanism of glucose sensing in mammalian cells remains to be elucidated. We have reported glucose deprivation rapidly induces AKT phosphorylation through PI3K activation. We assumed that regulation of AKT is relevant to glucose sensing and further investigated the underlying mechanisms. In this study, AKT phosphorylation under glucose deprivation was inhibited by galactose and fructose, but induced by 2-deoxyglucose (2-DG). Both 2-DG treatment and glucose deprivation were found to induce AKT phosphorylation in HepG2 cells. These findings suggested that glucose transporter may not be involved in the sensing of glucose and induction of AKT phosphorylation, and that downstream metabolic events may have important roles. A variety of metabolic stresses reportedly induce the production of reactive oxygen species (ROS). In the present study, glucose deprivation was found to induce intracellular hydrogen peroxide (H_2O_2) production in HepG2 cells. N-acetylcysteine (NAC), an antioxidant reagent, reduced both the increase in cellular H_2O_2 levels and AKT phosphorylation induced by glucose deprivation. These results strongly suggest that the glucose deprivation-induced increase of H_2O_2 in the cells mediated the AKT phosphorylation. RNA interference of NOX4, but not of NOX5, completely suppressed the glucose deprivation-induced AKT phosphorylation as well as increase of the intracellular levels of ROS, whereas exogenous H_2O_2 could still induce AKT phosphorylation in the NOX4-knockdown cells. In this study, we demonstrated that the ROS generated by NOX4 are involved in the intracellular adaptive responses by recognizing metabolic flux.

Citation: Owada S, Shimoda Y, Tsuchihara K, Esumi H (2013) Critical Role of H_2O_2 Generated by NOX4 during Cellular Response under Glucose Deprivation. PLoS ONE 8(3): e56628. doi:10.1371/journal.pone.0056628

Editor: Junji Yodoi, Institute for Virus Research, Laboratory of Infection and Prevention, Japan

Received October 1, 2012; **Accepted** January 11, 2013; **Published** March 21, 2013

Funding: This work was supported by a Grant for the 3rd Term Comprehensive 10-Year Strategy for Cancer Control from the Ministry of Health, Labour and Welfare Japan [H22-3ji taigann-ippann-033 to HE] (http://www.mhlw.go.jp/english/). No additional external funding received for this study. The funders had no role in study design, data collection and analysis, decision to publish, or preparation of the manuscript.

Competing Interests: The authors have declared that no competing interests exist.

* E-mail: hesumi@ncc.go.jp

Introduction

The supply of nutrients and oxygen is pivotal for cell survival and function, because of the large energy requirements of cells. This need is especially critical during cell proliferation. Proliferation is a process during which the numbers of cells successively double; therefore, the synthesis of nucleic acids, lipids, proteins and sugars is obligatory for successful proliferation. Glucose serves as a carbon source for the synthesis of nucleic acids, non-essential amino acids, lipids, and sugar. The intermediate metabolites in the glycolytic system are indispensable for non-essential amino acid synthesis, and intermediate metabolites and coenzymes in the pentose-5-phosphate pathway are required for the synthesis of nucleic acids and lipids. In addition, glucose is also needed for energy production in all cells.

Because of the pivotal role of glucose in the maintenance of the cellular functions, survival, and proliferation, elaborate mechanisms for detecting glucose availability in the cellular microenvironment exist in cells. The molecular mechanisms involved in the sensing of extracellular glucose concentrations have been extensively studied in yeasts. Yeasts detect the extracellular glucose concentrations using Snf3/Rtg2 (a glucose transporter homolog that has no capability as a transporter). Extracellular glucose causes this sensor to generate an intracellular signal that induces the expressions of several HXT genes encoding hexose transporters. The glucose signal induces HXT gene expression by influencing the function of the Rgt1 transcriptional repressor. In the absence of glucose, Rgt1 is functional and binds to the promoters of the HXT genes, repressing their functions [1,2,3]. In contrast, the biochemical basis of the glucose sensing mechanism in mammalian cells is largely unknown.

Meanwhile, most of human cancer tissues are known to be hypoxic, the hypoxia being caused mainly by a poor and heterogeneous blood supply [4,5,6,7]. Glucose as well as oxygen is supplied to cancer tissues via the blood stream, and we assumed that the glucose supply might be limited in human cancer tissues. In fact, the glucose concentrations in human colon cancer and gastric cancer tissues were found to be significantly lower than those in surrounding non-cancerous tissues [8]. In the cancer cells that exist in such environments, the monitoring of and adaptation to extracellular glucose concentrations are assumed to be important for the survival/proliferation of the tumor cells. We previously reported that AKT phosphorylation is immediately enhanced by the absence of glucose and plays a critical role in

cellular survival under such condition in various cell lines [9,10]. AKT can also be activated in response to a variety of cellular stresses, such as heat shock, ultraviolet light irradiation, ischemia, hypoxia, hyperglycemia, and oxidative stress. AKT is a serine and threonine kinase that mediates cell survival under these aforementioned conditions [11,12,13,14,15].

In the present study, we attempted to elucidate the molecular and biochemical mechanisms involved in the sensing of mammalian cells of the extracellular glucose concentrations, using AKT phosphorylation as an index of the cellular responses to glucose deprivation. We demonstrate the contribution of the H_2O_2 generated by NOX4 in the cellular sensing of and adaptation to poor glucose supply.

Materials and Methods

Cell cultures

Human fibroblasts derived from the subserosa of the stomach used for this study were kindly gifted to us by Dr Atsushi Ochiai (Pathology Division, Research Center for Innovative Oncology, National Cancer Center Hospital East). Human pancreatic cancer cells (PANC-1), human hepatocellular carcinoma cells (HepG2) and human fibroblasts derived from subserosa of the stomach were cultured in DMEM (GIBCO) supplemented with 10% fetal bovine serum (Biowest). All the cells were purchased from ATCC. The glucose-deprived condition was created as described previously [16].

Reagents

2′, 7′- Dichlorodihydrofluorescin diacetate (DCFDA) was purchased from Invitrogen. 3′-O-Acetyl-6′-O-pentafluorobenzenesulfonyl-2′,7′-difluorofluorescein (Bes-H_2O_2), galactose and fructose were purchased from Wako Pure Chemical Industries. N-acetyl-L-cysteine (NAC) and 2-deoxy-D-glucose (2-DG) were purchased from Sigma Aldrich. LY294002 and PP2 were purchased from Calbiochem.

Immunoblot analyses

Cells were homogenized in lysis buffer containing 10% SDS (sodium dodecyl sulfate), 10 mM Tris-HCl (pH 7.5) and 1 mM sodium orthovanadate, as described previously [17], and subjected to SDS-PAGE (SDS polyaclylamide gel electrophoresis). The proteins were transferred to a polyvinylidene fluoride microporous membrane (Millipore). The primary antibodies used were: anti-phospho-AKT Ser-473, anti-phospho-SRC Family Tyr-416, and anti-AKT, all obtained from Cell Signaling Technologies, and anti-actin (sc-1615), and c-SRC antibody (SRC2), obtained from Santa Cruz Biotechnology. The anti-OSSA antibody was a kind gift from Dr. Ryuuichi Sakai, National Cancer Center Research Institute. The following secondary antibodies were purchased from Santa Cruz Biotechnology: goat anti-mouse IgG-HRP, goat anti-rabbit IgG-HRP. The immunoblots were scanned using a CanoScan LiDE60 image scanner (Canon).

siRNA transfection

OSSA, NOX4, NOX5, and non-targeting siRNA were purchased from Invitrogen. For the siRNA experiments, the cells were transfected separately using a non-targeting siRNA or two separate specific siRNAs using Lipofectamine 2000 (Invitrogen).

RT-PCR

Total RNAs were prepared from the cells using ISOGEN (Nippon Gene), and reverse transcription was performed using superscript VILO (Invitrogen). PCR for human NOX family genes was carried out using the following primers: forward 5′-CTCAGCGGAATCAATCAGCTGTG-3′ and reverse 5′-AGAGGAACACGACAATCAGCCTTAG-3′ for Nox4; forward 5′-ATCAAGCGGCCCCCTTTTTTTCAC-3′ and reverse 5′-CTCATTGTCACACTCCTCGACAGC-3′ for Nox5.

Measurement of intracellular ROS levels

The cells were treated under various conditions and then incubated in DMEM or glucose-deprived medium containing 5 μM of DCFDA or 5 μM BES-H_2O_2-Ac at 37°C for 30 min. Then, the cells were detached from the plate with trypsin/EDTA, washed with PBS, resuspended in 500 μL of PBS, and placed on ice, protected from light. The intensity of the fluorescence of each cell was immediately measured using a FACS CANTO (Becton Dickinson) equipped with an argon ion laser (488 nm excitation). Each experiment was conducted in triplicate, and 10,000 cells per sample were measured. The histogram was analyzed using the software program BD FACS DIVA (Becton Dickinson).

Results

AKT activation by glucose deprivation

Within 30 minutes, and still after 3 hours, of transferring the HepG2 cells from ordinary DMEM to glucose-deprived medium, AKT was strongly phosphorylated at Ser 473; furthermore, AKT phosphorylation was significantly inhibited by treatment with LY294002 [18], an inhibitor of PI3K (Fig. 1A). Similarly, PI3K-dependent AKT activation was also observed in the pancreatic PANC-1 cells (Fig. S1) in a previous study [10]. Furthermore, increase of AKT phosphorylation induced by glucose deprivation was also observed in human fibroblasts derived from the subserosa of the stomach (Fig. S2).

To examine how glucose deprivation is recognized in these cells, concentration-dependent AKT activation in response to glucose deprivation was examined. When the HepG2 cells were exposed to media containing less than 1.38 mM of glucose, corresponding to one-quarter of the blood glucose level, AKT activation was clearly observed (Fig. 1B). Similarly, an increase in AKT phosphorylation was also observed in PANC-1 cells cultured in the presence of glucose at concentrations of less than 0.69 mM (Fig. S3). To elucidate the glucose sensing mechanism of the cells, the effect of glucose analogues on the AKT activation in response to glucose deprivation was examined. AKT activation was completely inhibited by the addition of either galactose or fructose at a final concentration of 5.5 mM (Fig. 1C). Similar results were observed in the PANC-1 cells (Fig. S4). These observations indicate that AKT is activated by a decrease of some metabolites of glycolysis or metabolic stress, rather than by the decrease of glucose itself. In yeast, the extracellular glucose concentration is sensed by a glucose transporter [1,2,3]. To examine whether a similar mechanism may also prevail in mammalian cells, the influence of 2-DG [19,20] on the AKT phosphorylation induced by glucose deprivation was examined. As shown in Fig. 1D, AKT phosphorylation in the HepG2 cells in response to glucose deprivation was not inhibited by 2-DG. Rather, AKT phosphorylation was clearly induced by the addition of 5.5 mM 2-DG, even in the presence of glucose. This observation indicates that glucose is not sensed by binding to a receptor or transporter, nor is it sensed by hexokinase, because 2-DG can be phosphorylated as efficiently by mammalian hexokinase as glucose. It is possible that the inhibition of binding of some sensors to glucose, if such an interaction occurs, might evoke the same cellular responses as glucose deprivation.

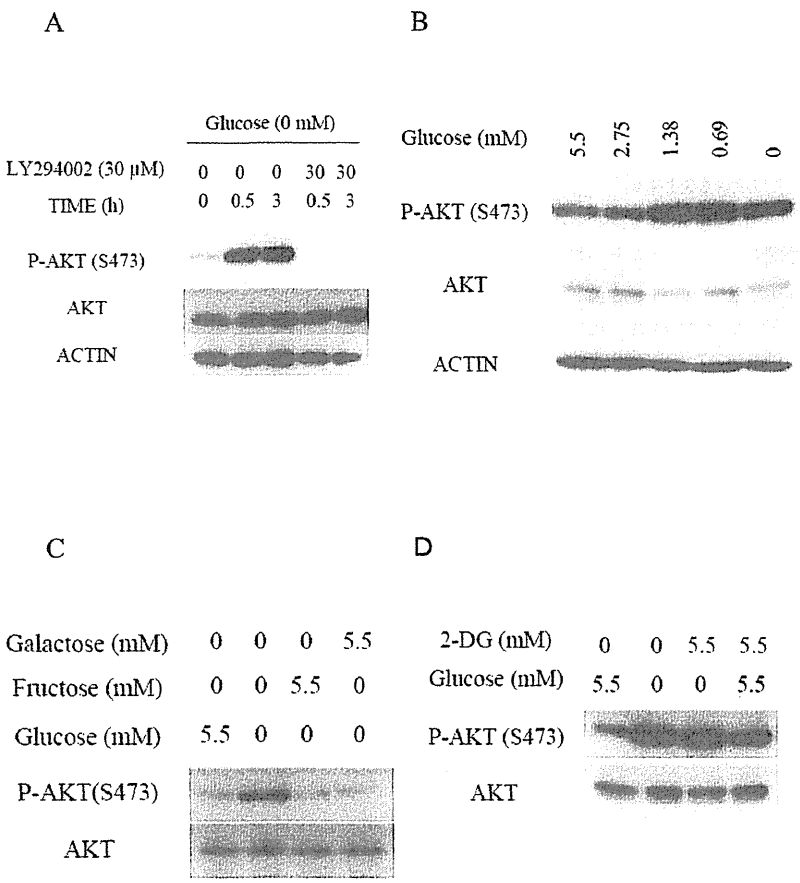

Figure 1. AKT phosphorylation was induced under glucose deprivation. (A) Immunoblotting analyses after incubation of HepG2 cells in the absence or presence of 5.5 mM of glucose and absence or presence of 30 μM of LY294002 for the indicated times. (B) HepG2 cells treated or not treated with various concentrations of glucose for 0.5 h were subjected to immunoblotting. (C) Immunoblotting analyses of HepG2 cells treated or not treated with 5.5 mM of glucose, 5.5 mM of galactose, or 5.5 mM of fructose for 0.5 h. (D) Immunoblotting analyses of HepG2 cells treated or not treated with 5.5 mM of glucose, 5.5 mM of 2-DG, or 5.5 mM of glucose plus 5.5 mM of 2-DG for 0.5 h.
doi:10.1371/journal.pone.0056628.g001

Role of hydrogen peroxide in the activation of AKT in response to glucose deprivation

Since AKT phosphorylation in response to glucose deprivation was attenuated by galactose, we assumed that changes in the metabolism might be the cause of the increase in AKT activation. Reactive oxygen species (ROS) are reportedly produced in cells under metabolic stresses [21,22]. We evaluated the intracellular levels of ROS using dichlorofluorescein diacetate (DCFDA), which measures hydroxyl and peroxyl radicals and other ROS. A significant increase in the intracellular ROS production was observed in the HepG2 cells cultured in glucose-deprived medium treated with DCFDA for 30 minutes (Fig. 2A). 3′-O-acetyl-6′-O-pentafluorobenzenesulfonyl- 2′,7′-difluorofluorescein (BES-H_2O_2) specifically detects an increase in the amounts of hydrogen peroxide (H_2O_2) [23] in cells treated under the same conditions (Fig. 2B). An increase in the production of ROS induced by glucose deprivation was also observed in the PANC-1 cells and human fibroblasts derived from the subserosa of the stomach (Fig. S5,S6). Addition of galactose or fructose completely prevented the H_2O_2 increase (Fig. S7). These results clearly showed that H_2O_2 production is induced by glucose deprivation. To elucidate the causal relationship between H_2O_2 production and AKT phosphorylation, the effect of addition of exogenous H_2O_2 on AKT phosphorylation was examined. Exogenous H_2O_2 addition to the culture medium induced PI3K-dependent AKT phosphorylation in a manner similar to glucose deprivation (Fig. 2C). To confirm the causal relation further, the influence of N-acetylcysteine (NAC), an antioxidant reagent, on the AKT phosphorylation induced in the absence of glucose was examined. The addition of NAC to the culture medium at a final concentration of 12.5 mM markedly reduced the ROS levels even under glucose-deprived conditions (Fig. 2A and 2B). Furthermore, the NAC treatment also suppressed the AKT phosphorylation induced by glucose deprivation (Fig. 2D).

SRC and OSSA are indispensable for AKT phosphorylation induced by glucose deprivation

SRC is involved in an alternate PI3K-activating pathway, and OSSA, a scaffold protein also known as FAM120A, reportedly activates the SRC-PI3K pathway in the presence of oxidative stress [24]. Thus, the involvements of SRC and OSSA in the glucose deprivation-induced phosphorylation of AKT were examined. PP2, a specific SRC family inhibitor [25], clearly inhibited the AKT phosphorylation induced by glucose deprivation (Fig. 3A). PP2 also inhibited AKT phosphorylation induced by exogenous H_2O_2 (Fig. 3B). Consistent with these findings, PP2

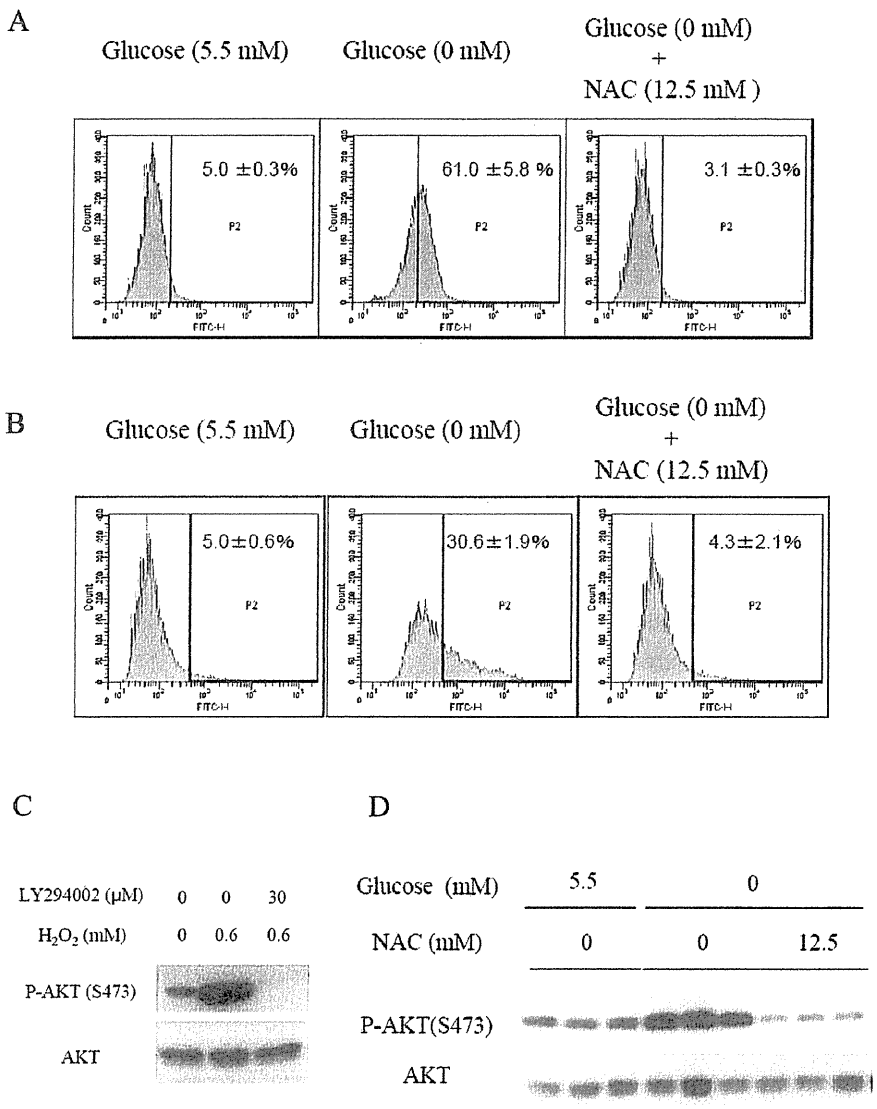

Figure 2. ROS mediates AKT phosphorylation under glucose deprivation. (A)(B)(D) HepG2 cells were cultured in either glucose-containing medium or glucose-deprived medium in the absence or presence of 12.5 mM of NAC for 0.5 h. ROS production was measured using flow cytometry. Cells were stained with (A) 5 μM of DCFDA or (B) 5 μM of BES-H_2O_2. Cells were gated within a range contained in the upper 5% of the total cell count under the glucose replete condition. (D) The AKT phosphorylation level was evaluated by immunoblotting. (C) Addition of H_2O_2 to media containing 5.5 mM of glucose in the absence or presence of 30 μM of LY294002 for 0.5 h, followed by immunoblotting.
doi:10.1371/journal.pone.0056628.g002

also suppressed the phosphorylation of SRC induced by glucose deprivation and exogenous H_2O_2 (Fig. S8). PP2 treatment did not alter the increased ROS levels in HepG2 cells cultured under glucose-deprived conditions (Fig. 3C). Similarly, LY294002 treatment inhibited AKT phosphorylation, but did not alter the ROS production (Fig. 1A, 3C). Suppression of OSSA expression by RNA interference inhibited the AKT phosphorylation induced by glucose deprivation and exogenous H_2O_2 (Fig. 3D, 3E and 3F). Thus, SRC and OSSA were concluded as being mediators of the H_2O_2 signals induced by glucose deprivation that activate the PI3K-AKT axis.

NOX4 knockdown inhibits hydrogen peroxide generation under glucose-deprived conditions

NOX4, one of the members of the NADPH oxidase family, is known to be closely involved in the production of ROS in response to growth factor stimuli [26]. Thus, its involvement also in glucose deprivation-induced AKT phosphorylation was examined. RNA interference selectively reduced the expression of NOX4 in HepG2 cells (Fig. 4A). Increase of intracellular ROS levels by glucose deprivation was suppressed by NOX4 knockdown (Fig. 4B). Consistent with this finding, AKT phosphorylation was also not induced in the NOX4 knockdown cells, while exogenous H_2O_2 clearly induced AKT phosphorylation in the cells (Fig. 4C). Similar results were obtained in the PANC-1 cells (Fig. S9A, B). PANC-1 cells express NOX5 as well as NOX4, however,

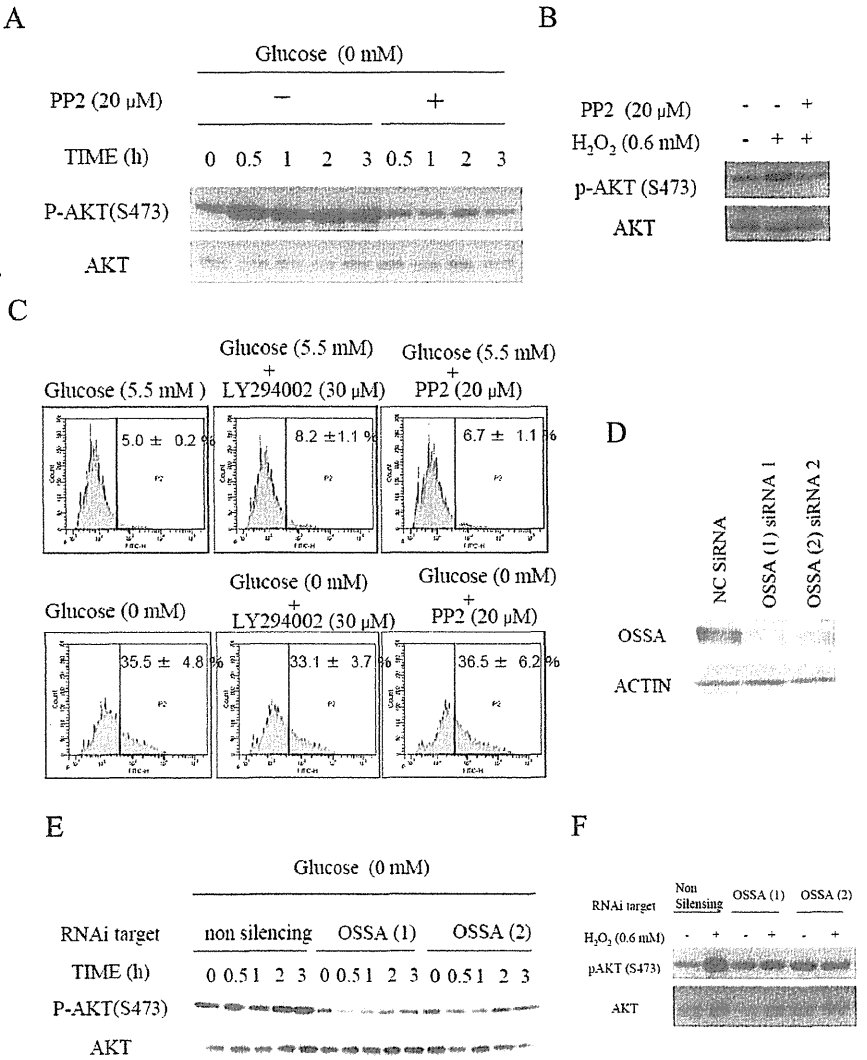

Figure 3. SRC and OSSA are indispensable for the AKT phosphorylation induced by glucose deprivation. (A) Immunoblotting analyses of HepG2 cells in the absence or presence of 5.5 mM of glucose in the and absence or presence of 20 μM of PP2 for the indicated times. (B) Addition of H_2O_2 to the culture medium containing 5.5 mM glucoseln the absence or presence of 20 μM of PP2 for 0.5 h, followed by immunoblotting. (C) HepG2 cells were cultured in medium containing or not containing (glucose-deprived) 5.5 mM of glucose in the absence or presence of 30 μM of LY204002 or 20 μM of PP2 for 0.5 h. The cells were stained with 5 μM of BES-H_2O_2. ROS production was measured using flow cytometry. (D) siRNA-treated HepG2 cells were subjected to immunoblotting analyses using OSSA antibody. (E) Immunoblotting analyses of HepG2 cells transfected with a non-targeting siRNA or two separate OSSA siRNAs in the absence or presence of 5.5 mM of glucose for the indicated times. (F) Addition of H_2O_2 to the medium of OSSA-knockdown cells containing 5.5 mM glucose for 0.5 h, followed by immunoblotting.
doi:10.1371/journal.pone.0056628.g003

knockdown of NOX5 did not alter the AKT phosphorylation level (Fig. S10A, B).

Discussion

In this study, we tried to elucidate the mechanism of sensing of the extracellular glucose concentration by cells, using AKT phosphorylation as a marker. As reported previously, AKT phosphorylation is induced by glucose deprivation [9,10]. In addition, increase in AKT phosphorylation has also been confirmed in HepG2 cells cultured in media containing one-quarter of the normal physiological glucose concentration. This fact suggests that cells have sophisticated mechanisms for monitoring extracellular glucose levels. In another study, increase in AKT phosphorylation was confirmed in PANC-1 cells cultured in the presence of glucose levels that are one-eighth of the normal physiological condition. The difference in the minimal trigger concentration of glucose between the HepG2 cells and PANC-1 cells could be related to differences in the origins of the cells or differences in the microenvironments of the tumors the cells were derived from.

In the present study, increase in ROS production was observed by 30 minutes after glucose deprivation, both in cancer cells and human fibroblasts. Thus, it became evident that the mechanism of ROS production under glucose deprivation is preserved in not only cancer cells, but also human fibroblasts. ROS was strongly suspected to mediate the AKT phosphorylation, because AKT

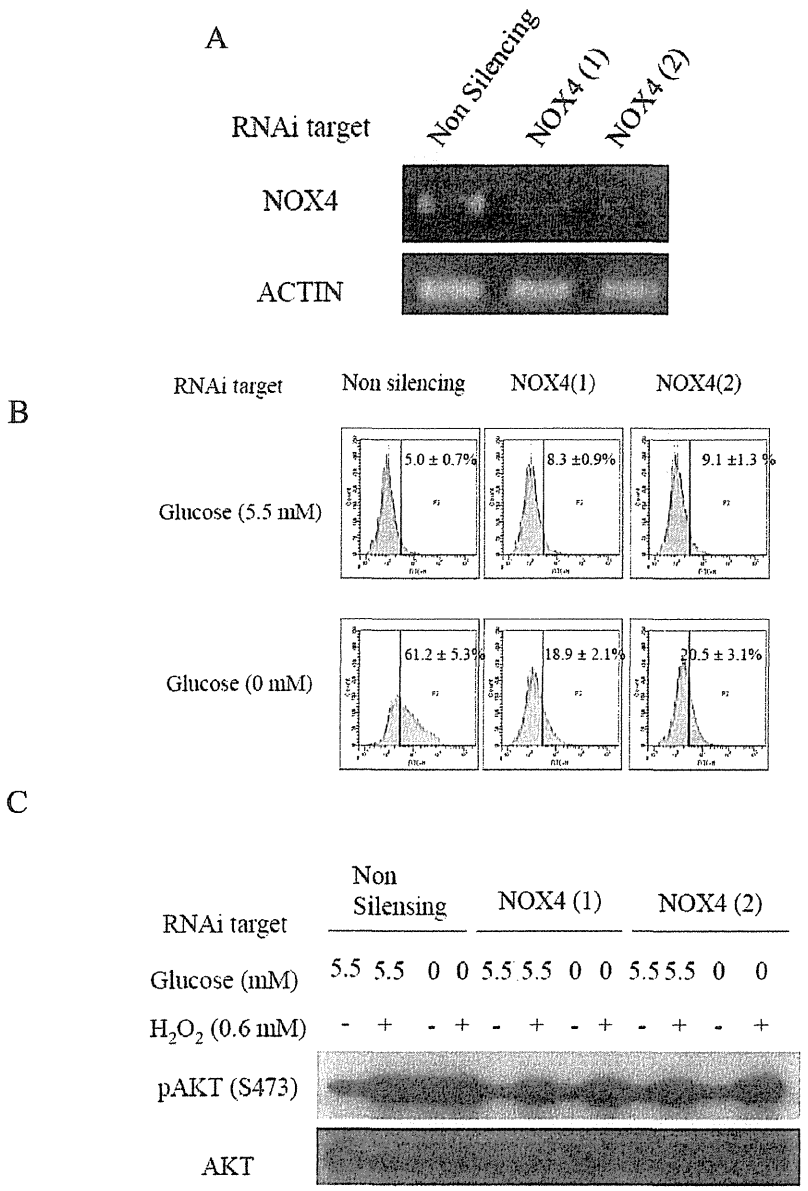

Figure 4. Induction of AKT phosphorylation under glucose deprivation is mediated by ROS generated by NOX4. (A) *siRNA*-treated HepG2 cells were subjected to reverse-transcriptase PCR (RT-PCR) to confirm NOX4 knockdown. (B) NOX4 knockdown HepG2 Cells were stained with 5 μM of BES-H_2O_2 in the absence or presence of 5.5 mM of glucose for 0.5 h. ROS production was measured using flow cytometry. (C) Immunoblotting analyses of HepG2 cells transfected with a non-targeting siRNA or two separate NOX4 siRNAs in the absence or presence of 5.5 mM of glucose or treatment with exogenous H_2O_2 for 0.5 h.
doi:10.1371/journal.pone.0056628.g004

phosphorylation was inhibited by treatment with NAC. As H_2O_2 has a low selectivity for downstream molecules, it may be involved in the regulation of numerous signaling pathways [27,28,29]. Among them, the regulation of AKT phosphorylation, as reported here, is particularly intriguing. AKT mediates cell proliferation and survival [30,31]. In our previous work, Akt activation was found to play a critical role in cell survival under glucose deprivation [10]. Furthermore, OSSA knockdown and the inhibition of SRC by PP2 suggests that these two elements are fundamental to AKT phosphorylation induced by glucose deprivation. It has been reported that SRC family kinases as their redox sensitive cysteines are the targets of specific oxidation by various oxidants, including H_2O_2 [32]. In this study, we clarified that PP2, a specific SRC inhibitor, inhibited AKT phosphorylation induced by glucose deprivation and exogeneous hydrogen peroxide. Thus, SRC is a strong candidate as a hydrogen peroxide sensor. Since PP2 inhibits SRC and other members of the SRC family, we should be careful before denying the relevance of other SRC family kinases [25]. Further investigations, such as by knockdown of individual SRC family kinases will be needed to identify the relevant Src-family kinase.

As with most intracellular signaling cascades, cross-talk and feedback interactions contribute to the overall regulation of PI3K/AKT signaling. S6 kinase-1, a downstream effector of mTORC1,

is known to be involved in a negative feedback loop of AKT activation. S6 kinase phosphorylates and inhibits upstream insulin receptor substrate proteins, which diminishes signaling through the PI3K/AKT pathway [33]. We observed that S6 kinase-1 phosphorylation was suppressed in PANC-1 cells under glucose deprivation (unpublished data), suggesting that the negative feedback machinery could be another mechanism regulating AKT phophorylation in cells under glucose deprivation. Furthermore, it was considered that the NADPH/NADP and ATP/AMP ratios may possibly change under glucose deprivation. Therefore, we measured the NADPH/NADP and ATP/AMP ratios; however, no significant changes were observed in at least the first 30 minutes. We also examined the effect of AMPK activation induced by AICAR on AKT activation and the cellular levels of hydrogen peroxide level, but again no significant changes were observed (unpublished data).

AKT phosphorylation in response to glucose deprivation was also completely inhibited following the addition of galactose or fructose instead of glucose. Galactose and fructose enter the glycolytic pathway after they have been metabolized intracellularly to glucose-6-phosphate and fructose-1 or 6-phosphate, respectively. Therefore, the contribution of decrease in metabolites downstream of fructose-1 or 6-phosphate to the induction of AKT phosphorylation under glucose deprivation was hypothesized.

To examine the contribution of the mitochondria, which are the major loci of ROS production, PANC-1 Rho^0 cells depleted of mitochondrial DNA were produced. When the Rho^0 cells were exposed to glucose-deprived medium, a large amount of intracellular H_2O_2 was produced. As pyruvic acid alone did not inhibit the ROS production completely, we could not assess the contribution of the mitochondria to the induction of ROS production by glucose deprivation further by this method (Shimoda et al. unpublished data). We then studied the involvement of NOX4 as another major locus of ROS production. AKT phosphorylation induced by glucose deprivation was not observed after NOX4 knockdown; no increase in the intracellular ROS levels was observed either, indicating the involvement of NOX4 in the intracellular accumulation of ROS. The contribution of NOX4, but not NOX5, in the signaling triggered by glucose deprivation was rather unexpected. Interestingly, a previous study reported that NOX4 regulates the survival of PANC-1 cells via ROS/ASK1/AKT signaling [34]. It might also be involved in cell survival under glucose-deprived conditions. With respect to the regulation of their activities, there are fundamental differences among the NOX isoforms. Most NOX family members are reportedly switched on and off by their regulatory subunits. NOX4 also functions as a complex with p22phox on internal membranes to produce ROS [35,36]. NOX4, unlike other members of the NOX family, is known to constitutively induce the production of large amounts of H_2O_2, however, the possibility of growth factor signaling being mediated by NOX4 has also been suggested [37]. The results of the present study also suggested that the activity of NOX4 might be regulated. In the present study, glucose deprivation increased the cellular levels of H_2O_2, which was suppressed by frucotose and galactose, indicating that NOX4 might be activated by deprivation of some glycolytic intermediate or some downstream products, such as of the pentose phosphate shunt and/or TCA cycle. The results obtained with the use of 2-DG are consistent with this idea. Whether the ROS accumulation under glucose deprivation is caused by increased production of ROS as a result of enhanced activity of NOX4, or by decreased antioxidant capacity, such as that associated with deficient activities of catalase, glutathione peroxidase, and glutathione needs to be further investigated. The intracellular amount of ROS is determined by the activity of the enzymes and the amounts of the substrates available. Therefore, metabolomic analysis of the entire set of metabolites is desired.

In the present study, we found that cells sense and respond to metabolic flux rather than glucose itself, and NOX4 and its product, ROS, play important roles in the cellular adaptive responses.

Supporting Information

Figure S1 Immunoblotting analyses after incubating PANC-1 cells in the absence or presence of 5.5 mM of glucose in the absence or presence of 30 μM of LY294002 for the indicated times.
(TIF)

Figure S2 Immunoblotting analyses after incubating human fibroblasts derived from subserossa of stomach in the absence or presence of 5.5 mM of glucose for 0.5 h.
(TIF)

Figure S3 PANC-1 cells were treated with or without various concentrations of glucose for 0.5 h.
(TIF)

Figure S4 Immunoblotting analyses after incubating PANC-1 cells in the absence or presence of 5.5 mM of glucose, 5.5 mM of galactose, or 5.5 mM of fructose for 0.5 h.
(TIF)

Figure S5 PANC-1 cells were cultured in either glucose-containing medium or glucose-deprived medium for 0.5 h. Cells were stained with 5 μM BES-H_2O_2. ROS production was measured using flow cytometry.
(TIF)

Figure S6 Human fibroblasts derived from subserossa of stomach were cultured in either glucose-containing medium or glucose-deprived medium for 0.5 h. Cells were stained with 5 μM BES-H_2O_2. ROS production was measured using flow cytometry.
(TIF)

Figure S7 HepG2 cells were cultured in the absence or presence of 5.5 mM of glucose, 5.5 mM of galactose, or 5.5 mM of fructose for 0.5 h. ROS production was measured using flowcytometry. Cells were stained with 5 μM of BES-H_2O_2.
(TIF)

Figure S8 Immunoblotting analyses of HepG2 cells in the absence or presence of 5.5 mM of glucose or treatment with exogenous H_2O_2 for 0.5 h.
(TIF)

Figure S9 (A) siRNA-treated PANC-1 cells were subjected to reverse transcriptional PCR (RT-PCR) to confirm NOX4 knockdown. (B) Immunoblotting analyses after incubating PANC-1 cells transfected with a non-targeting siRNA or two separate NOX4 siRNA in the absence or presence of 5.5 mM of glucose for 0.5 h.
(TIF)

Figure S10 (A) siRNA-treated PANC-1 cells were subjected to reverse transcriptional PCR (RT-PCR) to confirm NOX5 knockdown. (B) Immunoblotting analyses after incubating

PANC-1 cells transfected with a non-targeting siRNA or two separate NOX5 siRNA in the absence or presence of 5.5 mM of glucose for 0.5 h.
(TIF)

Acknowledgments

We thank Dr. Ryuichi Sakai (National Cancer Center Research Institute) for kindly gifting the OSSA antibody.

We thank Dr. Atsushi Ochiai (Pathology Division, Research Center for Innovative Oncology, National Cancer Center Hospital East) for kindly gifting the primary human stomach subserosal fibroblasts.

Author Contributions

Conceived and designed the experiments: SO HE KT. Performed the experiments: SO YS. Analyzed the data: SO YS. Wrote the paper: SO HE KT.

References

1. Flick KM, Spielewoy N, Kalashnikova TI, Guaderrama M, Zhu QZ, et al. (2003) Grr1-dependent inactivation of Mth1 mediates glucose-induced dissociation of Rgt1 from HXT gene promoters. Mol Biol Cell 14: 3230–3241.
2. Kim JH, Polish J, Johnston M (2003) Specificity and regulation of DNA binding by the yeast glucose transporter gene repressor Rgt1. Mol Cell Biol 23: 5208–5216.
3. Ozcan S, Johnston M (1999) Function and regulation of yeast hexose transporters. Microbiol Rev 63: 554–569.
4. Brown JM, Giaccia AJ (1998) The unique physiology of solid tumors: Opportunities (and problems) for cancer therapy. Cancer Res 58: 1408–1416.
5. Jain RK (2003) Molecular regulation of vessel maturation. Nat Med 9: 685–693.
6. Less JR, Skalak TC, Sevick EM, Jain RK (1991) Microvascular Architecture in a Mammary-Carcinoma - Branching Patterns and Vessel Dimensions. Cancer Res 51: 265–273.
7. Thomlinson RH, Gray LH (1955) The histological structure of some human lung cancers and the possible implications for radiotherapy. Br J Cancer 9: 539–49.
8. Hirayama A, Kami K, Sugimoto M, Sugawara M, Toki N, et al. (2009) Quantitative Metabolome Profiling of Colon and Stomach Cancer Microenvironment by Capillary Electrophoresis Time-of-Flight Mass Spectrometry. Cancer Res 69: 4918–4925.
9. Esumi H, Lu J, Kurashima Y, Hanaoka T (2004) Antitumor activity of pyrvinium pamoate, 6-(dimethylamino)-2- 2-(2,5-dimethyl-1-phenyl-1H- pyrrol-3-yl)ethenyl -1-methyl-quinolinium pamoate salt, showing preferential cytotoxicity during glucose starvation. Cancer Sci 95: 685–690.
10. Izuishi K, Kato K, Ogura T, Kinoshita T, Esumi H (2000) Remarkable tolerance of tumor cells to nutrient deprivation: Possible new biochemical target for cancer therapy. Cancer Res 60: 6201–+.
11. Alvarez-Tejado M, Alfranca A, Aragones J, Vara A, Landazuri MO, et al. (2002) Lack of evidence for the involvement of the phosphoinositide 3-kinase/Akt pathway in the activation of hypoxia-inducible factors by low oxygen tension. J Biol Chem 277: 13508–13517.
12. Bang OS, Ha BG, Park EK, Kang SS (2000) Activation of Akt is induced by heat shock and involved in suppression of heat-shock-induced apoptosis of NIH3T3 cells. Biochem Biophys Res Commun 278: 306–311.
13. Esposito F, Chirico G, Gesualdi NM, Posadas I, Ammendola R, et al. (2003) Protein kinase B activation by reactive oxygen species is independent of tyrosine kinase receptor phosphorylation and requires Src activity. J Biol Chem 278: 20828–20834.
14. Jiang ZJ, Zhang Y, Chen XQ, Lam PY, Yang H, et al. (2002) Activation of Erk1/2 and Akt in astrocytes under ischemia. Biochem Biophys Res Commun 294: 726–733.
15. Nomura M, Kaji A, Ma WY, Zhong SP, Liu GM, et al. (2001) Mitogen and stress-activated protein kinase 1 mediates activation of Akt by ultraviolet B irradiation. J Biol Chem 276: 25558–25567.
16. Tomitsuka E, Kita K, Esumi H (2012) An anticancer agent, pyrvinium pamoate inhibits the NADH-fumarate reductase system a unique mitochondrial energy metabolism in tumour microenvironments. J Biochem 152: 171–83.
17. Inazuka F, Sugiyama N, Tomita M, Abe T, Shioi G, et al. (2012) Muscle-specific Knock-out of NUAK Family SNF1-like Kinase 1 (NUAK1) Prevents High Fat Diet-induced Glucose Intolerance. J Biol Chem 287: 16379–16389.
18. Guo M, Joiakim A, Reiners JJ (2000) Suppression of 2,3,7,8-tetrachlorodibenzo-p-dioxin (TCDD)-mediated aryl hydrocarbon receptor transformation and CYP1A1 induction by the phosphatidylinositol 3-kinase inhibitor 2-(4-morpholinyl)-8-phenyl-4H-1-benzopyran-4-one (LY294002). Biochemical Pharmacol 60: 635–642.
19. Crane RK, Sols A (1954) The non-competitive inhibition of brain hexokinase by glucose-6-phosphate and related compounds. J Biol Chem 210: 597–606.
20. Tower DB (1958) The effects of 2-deoxy-D-glucose on metabolism of slices of cerebral cortex incubated in vitro. J Neurochem 3: 185–205.
21. Liu L, Wise DR, Diehl JA, Simon MC (2008) Hypoxic Reactive Oxygen Species Regulate the Integrated Stress Response and Cell Survival. J Biol Chem 283: 31153–31162.
22. Bensaad K, Cheung EC, Vousden KH (2009) Modulation of intracellular ROS levels by TIGAR controls autophagy. EMBO J 28: 3015–3026.
23. Maeda H, Futkuyasu Y, Yoshida S, Fukuda M, Saeki K, et al. (2004) Fluorescent probes for hydrogen peroxide based on a non-oxidative mechanism. Angew Chem Int Ed 43: 2389–2391.
24. Tanaka M, Sasaki K, Kamata R, Hoshino Y, Yanagihara K, et al. (2009) A Novel RNA-Binding Protein, Ossa/C9orf10, Regulates Activity of Src Kinases To Protect Cells from Oxidative Stress-Induced Apoptosis. Mol Cell Biol 29: 402–413.
25. Hanke JH, Gardner JP, Dow RL, Changelian PS, Brissette WH, et al. (1996) Discovery of a novel, potent, and Src family-selective tyrosine kinase inhibitor - Study of Lck- and FynT-dependent T cell activation. J Biol Chem 271: 695–701.
26. Xi G, Shen X, Maile LA, Wai C, Gollahon K, et al. (2012) Hyperglycemia Enhances IGF-I-Stimulated Src Activation via Increasing Nox4-Derived Reactive Oxygen Species in a PKC zeta-Dependent Manner in Vascular Smooth Muscle Cells. Diabetes 61: 104–113.
27. Aggeli I-KS, Gaitanaki C, Beis I (2006) Involvement of JNKs and p38-MAPK/MSK1 pathways in H2O2-induced upregulation of heme oxygenase-1 mRNA in H9c2 cells. Cell Signal 18: 1801–1812.
28. Kim YK, Bae GU, Kang JK, Park JW, Lee EK, et al. (2006) Cooperation of H2O2-mediated ERK activation with Smad pathway in TGF-beta 1 induction of p21(WAF1/Cip1). Cell Signal 18: 236–243.
29. Takada Y, Mukhopadhyay A, Kundu GC, Mahabeleshwar GH, Singh S, et al. (2003) Hydrogen peroxide activates NF-kappa B through tyrosine phosphorylation of I kappa B alpha and serine phosphorylation of p65 - Evidence for the involvement of I kappa B alpha kinase and Syk protein-tyrosine kinase. J Biol Chem 278: 24233–24241.
30. Burgering BMT, Coffer PJ (1995) Protein-Kinase-B (C-Akt) In Phosphatidylinositol-3-Oh Inase Signal-Transduction. Nature 376: 599–602.
31. Franke TF, Yang SI, Chan TO, Datta K, Kazlauskas A, et al. (1995) The Protein-Kinase Encoded by the Akt Protooncogene Is a Target of the Pdgf-Activated Phosphatidylinositol 3-Kinase. Cell 81: 727–736.
32. Giannoni E, Buricchi F, Raugei G, Ramponi G, Chiarugi P (2005) Intracellular reactive oxygen species activate Src tyrosine kinase during cell adhesion and anchorage-dependent cell growth. Mol Cell Biol 25: 6391–6403.
33. Tremblay F, Brule S, Um SH, Li Y, Masuda K, et al. (2007) Identification of IRS-1 Ser-1101 as a target of S6K1 in nutrient- and obesity-induced insulin resistance. Proc Natl Acad Sci U S A 104: 14056–14061.
34. Mochizuki T, Furuta S, Mitsushita J, Shang W, Ito M, et al. (2006) Inhibition of NADPH oxidase 4 activates apoptosis via the AKT/apoptosis signal-regulating kinase 1 pathway in pancreatic cancer PANC-1 cells. Oncogene 25: 3699–3707.
35. Sumimoto H, Miyano K, Takeya R (2005) Molecular composition and regulation of the Nox family NAD(P)H oxidases. Biochem Biophys Res Commun 338: 677–686.
36. Martyn KD, Frederick LM, von Loehneysen K, Dinauer MC, Knaus UG (2006) Functional analysis of Nox4 reveals unique characteristics compared to other NADPH oxidases. Cell Signal 18: 69–82.
37. Kim HJ, Kim C-H, Ryu J-H, Joo JH, Lee S-N, et al. (2011) Crosstalk between platelet-derived growth factor-induced Nox4 activation and MUC8 gene overexpression in human airway epithelial cells. Free Radic Biol Med 50: 1039–1052.

Metabolomics (2013) 9:444–453
DOI 10.1007/s11306-012-0452-2

ORIGINAL ARTICLE

Metabolomic profiling of lung and prostate tumor tissues by capillary electrophoresis time-of-flight mass spectrometry

Kenjiro Kami · Tamaki Fujimori · Hajime Sato · Mutsuko Sato · Hiroyuki Yamamoto · Yoshiaki Ohashi · Naoyuki Sugiyama · Yasushi Ishihama · Hiroko Onozuka · Atsushi Ochiai · Hiroyasu Esumi · Tomoyoshi Soga · Masaru Tomita

Received: 11 June 2012 / Accepted: 27 July 2012 / Published online: 2 November 2012

Abstract Metabolic microenvironment of tumor cells is influenced by oncogenic signaling and tissue-specific metabolic demands, blood supply, and enzyme expression. To elucidate tumor-specific metabolism, we compared the metabolomics of normal and tumor tissues surgically resected pairwise from nine lung and seven prostate cancer patients, using capillary electrophoresis time-of-flight mass spectrometry (CE-TOFMS). Phosphorylation levels of enzymes involved in central carbon metabolism were also quantified. Metabolomic profiles of lung and prostate tissues comprised 114 and 86 metabolites, respectively, and the profiles not only well distinguished tumor from normal tissues, but also squamous cell carcinoma from the other tumor types in lung cancer and poorly differentiated tumors from moderately differentiated tumors in prostate cancer. Concentrations of most amino acids, especially branched-chain amino acids, were significantly higher in tumor tissues, independent of organ type, but of essential amino acids were particularly higher in poorly differentiated than moderately differentiated prostate cancers. Organ-dependent differences were prominent at the levels of glycolytic and tricarboxylic acid cycle intermediates and associated energy status. Significantly high lactate concentrations and elevated activating phosphorylation levels of phosphofructokinase and pyruvate kinase in lung tumors confirmed hyperactive glycolysis. We highlighted the potential of CE-TOFMS-based metabolomics combined with phosphorylated enzyme analysis for understanding tissue-specific tumor microenvironments, which may lead to the development of more effective and specific anticancer therapeutics.

Keywords Metabolomics · CE-MS · Phosphoproteomics · Lung cancer · Prostate cancer · Tumor microenvironment

Kenjiro Kami and Tamaki Fujimori contributed equally to this study.

Electronic supplementary material The online version of this article (doi:10.1007/s11306-012-0452-2) contains supplementary material, which is available to authorized users.

K. Kami · Y. Ohashi · N. Sugiyama · T. Soga · M. Tomita
Institute for Advanced Biosciences, Keio University, Tsuruoka, Yamagata, Japan

K. Kami · T. Soga · M. Tomita
Systems Biology Program, Graduate School of Media and Governance, Keio University, Fujisawa, Kanagawa, Japan

T. Fujimori · H. Sato · M. Sato · H. Yamamoto · Y. Ohashi (✉) · T. Soga · M. Tomita
Human Metabolome Technologies, Inc., Tsuruoka, Yamagata, Japan
e-mail: ohashi@humanmetabolome.com

Y. Ishihama
Graduate School of Pharmaceutical Sciences, Kyoto University, Kyoto, Japan

H. Onozuka · A. Ochiai · H. Esumi (✉)
National Cancer Center Hospital East, Kashiwa, Chiba, Japan
e-mail: hesumi@ncc.go.jp

1 Introduction

Hyperactivity of glycolysis independent of oxygen availability is a hallmark of cancer metabolism (Warburg effect) (Warburg 1956). Glycolytic energy metabolism of tumor cells is advantageous for perpetual proliferation and meeting the high demand for non-essential amino acids, fatty acids, and nucleotides, although not for efficient production of ATP. Besides glucose, glutamine is significantly consumed by most tumor cells and metabolized to

alanine, lactate, and ammonium ions, which are secreted out of the cells, in a process called glutaminolysis (Heiden et al. 2009). Corroborating these features of cancer metabolism, our previous metabolome analyses of colon and stomach tumor tissues, using capillary electrophoresis time-of-flight mass spectrometry (CE-TOFMS), have revealed significantly high tumor concentrations of glycolytic intermediates including lactate, tricarboxylic acid (TCA) cycle intermediates, and amino acids (Hirayama et al. 2009). Moreover, inter-organ metabolomic differences were more significant than normal-versus-tumor differences within the same organ, which revealed the complexity in generalizing a tumor-specific, organ-independent metabolic profile. This suggested that cells alter their metabolism along with tumorigenesis while retaining much of the metabolism that is unique to their organs of origin. To test this hypothesis further and gain an insight into cancer metabolism, we analyzed metabolomic profiles of normal and tumor tissues obtained from lung and prostate cancer patients.

Deciphering the difference in the flow of energy metabolism between cancer and normal cells solely from the tissue metabolome data is often difficult. The activities of most glycolytic enzymes are known to be regulated by phosphorylation; therefore, we used nano-liquid chromatography-tandem mass spectrometry (nanoLC–MS/MS) to quantify phosphorylation levels of 13 sites contained in ten selected enzymes involved in glycolysis and the TCA cycle. The results indicate that tumor metabolomic profile is highly dependent on its organ of origin, and exhibits unique patterns dependent on cancer type as well as differentiation status. This demonstrates the potential of CE-TOFMS-based metabolomics complemented by phosphorylated enzyme analysis for gaining further insight into the complexity and heterogeneity of tumor metabolism.

2 Materials and methods

2.1 Sampling and metabolite extraction

All the experiments were conducted according to the study protocol that was approved by the Institution Review Board of the National Cancer Center, Japan. Informed consent was obtained from all the participants.

Tumor and surrounding tissues were surgically resected from nine lung and seven prostate cancer patients, who had been administered with no anticancer drugs or medications that could greatly modify their metabolisms previous to the surgical treatments. Clinical information on the patients is listed in Table 1. The resected tissue samples were immediately frozen in liquid nitrogen and stored at −80 °C until metabolite extraction. Sample tissues were weighed and completely homogenized by multi-beads shocker (Yasuikikai, Osaka, Japan) at 2,000 rpm for 3 min, after adding 0.5 ml ice-cold methanol containing 50 μM methionine sulfone and camphor-10-sulfonic acid as internal standards. The homogenates were mixed with 0.5 ml chloroform and 0.2 ml ice-cold Milli-Q water. After centrifugation at 2,300×*g* for 5 min, the supernatant was centrifugally filtrated through 5-kDa cut-off filters (Millipore, Bedford, MA, USA) at 9,100×*g* for 3 h to remove proteins. The filtrate was centrifugally concentrated in a vacuum evaporator, dissolved with Milli-Q water, and analyzed by CE-TOFMS.

Table 1 Clinicopathological information of patients and their tumor tissues. W, M, and P in the differentiation status indicate well-, moderately-, and poorly- differentiated tumors, respectively

Organ	ID	Age	Sex	Type	Stage	Differentiation
Lung	L1	82	Male	Squamous cell carcinoma	2B	M
	L2	82	Male	Squamous cell carcinoma	1B	M
	L3	77	Male	Squamous cell carcinoma	1B	P
	L4	80	Female	Adenocarcinoma	1B	M
	L5	78	Male	Pleomorphic carcinoma	3B	N/A
	L6	81	Male	Adenocarcinoma	1A	W
	L7	56	Male	Squamous cell carcinoma	3B	M–P
	L8	61	Male	Large cell carcinoma	1B	N/A
	L9	57	Male	Adenocarcinoma	1B	P
Prostrate	P1	68	Male	Adenocarcinoma	2	M
	P2	66	Male	Adenocarcinoma	2	P
	P3	67	Male	Adenocarcinoma	2	P
	P4	63	Male	Adenocarcinoma	3	P
	P5	62	Male	Adenocarcinoma	2	M
	P6	65	Male	Adenocarcinoma	2	M
	P7	58	Male	Adenocarcinoma	2	M

2.2 CE-TOFMS analysis and data processing

CE-TOFMS analysis was performed by an Agilent CE system combined with a TOFMS (Agilent Technologies, Palo Alto, CA, USA) as described previously (Ohashi et al. 2008) with slight modifications. Cationic metabolites were separated through a fused silica capillary (50 μm internal diameter × 80 cm total length) preconditioned with a commercial buffer (H3301-1001, Human Metabolome Technologies Inc. (HMT), Tsuruoka, Japan) and filled with 1 M formic acid as electrolyte, and a commercial sheath liquid (H3301-1020, HMT) was delivered at a rate of 10 μl/min. Sample solution was injected at a pressure of 50 mbar for 10 s. The applied voltage was set at 30 kV. Electrospray ionization-mass spectrometry (ESI-MS) was conducted in the positive-ion mode and the capillary and fragmentor voltages were set at 4,000 and 120 V, respectively. Nebulizer pressure was configured at 5 psig and N_2 was delivered as a drying gas at a rate of 7 l/min at 300 °C. Exact mass data were acquired at the rate of 1.5 cycles/s over a 50–1,000 *m/z* range. Anionic metabolites were analyzed also through the fused silica capillary preconditioned with a commercial buffer (H3302-1022, HMT) and filled with 50 mM ammonium acetate solution (pH 8.5) as electrolyte, and the aforementioned sheath liquid was delivered at a rate of 10 μl/min. Sample solution was injected at a pressure of 50 mbar for 6 s. The nebulizer pressure, drying gas and its flow rate, applied voltage, and scanning condition of the spectrometer were configured in the same manner as the cationic metabolite analysis. ESI-MS was conducted in the negative mode, and the capillary and fragmentor voltages were set at 3,500 and 125 V, respectively. The data obtained by CE-TOFMS analysis were preprocessed using our proprietary automatic integration software, MasterHands. Each metabolite was identified and quantified based on the peak information including *m/z*, migration time, and peak area. The quantified data were then evaluated for statistical significance by Wilcoxon signed-rank test.

2.3 Enrichment of phosphopeptides

Sample tissues were disrupted by multi-beads shocker and suspended in 100 mM Tris–HCl (pH 9.0) containing 8 M urea, protein phosphatase inhibitors and protein phosphatase inhibitors cocktails (Sigma, St. Louis, MO, USA). After centrifugation at 1,500×*g* for 10 min, the supernatant was reduced with 1 mM dithiothreitol, alkylated with 5 mM iodoacetamide, and then digested with Lys-C endopeptidase at 37 °C for 3 h, followed by 5-fold dilution with 50 mM ammonium bicarbonate and digestion with trypsin at 37 °C overnight. The digested samples were desalted using StageTips with SDB-XC Empore disk membranes (3 M, St. Paul, MN, USA) (Rappsilber et al. 2003).

Phosphopeptides were enriched with hydroxy acid-modified metal oxide chromatography (HAMMOC) (Kyono et al. 2008; Sugiyama et al. 2007). Briefly, custom-made metal oxide chromatography tips were prepared using C8-StageTips and titania beads as described previously (Rappsilber et al. 2007). Prior to loading samples, the tips were equilibrated with 0.1 % trifluoroacetic acid (TFA), 80 % acetonitrile and 300 mg/ml lactic acid (solution A). The digested samples from normal or tumor tissues were diluted with 100 μl solution A and loaded into the HAMMOC tips. After successive washing with solution A and solution B (0.1 % TFA and 80 % acetonitrile), 0.5 % piperidine was used for elution. The eluted fraction was acidified with TFA, desalted using SDB-XC-StageTips, and concentrated in a vacuum evaporator, followed by the addition of solution A for subsequent nanoLC–MS/MS analysis. The phosphopeptide enrichment and sample pretreatment was conducted in duplicate.

2.4 NanoLC–MS/MS analysis and database search

NanoLC–MS/MS analyses were conducted using LTQ-Orbitrap (Thermo Fisher Scientific, Rockwell, IL, USA), a Dionex Ultimate 3000 pump (Thermo Fisher Scientific) and an HTC-PAL autosampler (CTC Analytics, Zwingen, Switzerland). A self-pulled needle (150 mm length × 100 μm internal diameter, 6-μm opening) packed with ReproSil C18 materials (3 μm, Dr. Maisch, Ammerbuch, Germany) was used as an analytical column with "stone-arch" frit (Ishihama et al. 2002). A polytetrafluoroethylene-coated column holder (Nikkyo Technos, Tokyo, Japan) was mounted on an *x–y–z* nanospray interface, and a tee connector with a magnet was used to hold the column needle and to set the appropriate spray position. The injection volume was 5 μl and the flow rate was 500 nl/min for the gradient separation of peptides (Ishihama 2005). The mobile phases consisted of (A) 0.5 % acetic acid and (B) 0.5 % acetic acid and 80 % acetonitrile. A three-step linear gradient of 5–10 % B in 5 min, 10–40 % B in 60 min, 40–100 % B in 5 min and 100 % B in 10 min was used. A spray voltage of 2,400 V was applied via the tee connector. The MS scan range was *m/z* 300–1,500 and the top ten precursor ions were selected for subsequent MS/MS scans. Resolution setting and its maximum injection time were configured at 60,000 and 500 ms, respectively. We also configured the normalized collision energy at 35.0, the isolation width at two, and the minimum signal at 500. Automatic gain controls were set at 500,000 in the MS analysis and at 10,000 in the MS/MS analysis. The capillary temperature was set at 200 °C. A lock mass function was used with a peak derived from polydimethylsiloxane

as a lock mass for the LTQ-Orbitrap to obtain constant mass accuracy during gradient analysis (Olsen et al. 2005). Mass Navigator version 1.2 (Mitsui Knowledge Industry, Tokyo, Japan) was used to create peak lists on the basis of the recorded fragmentation spectra. Peptides and proteins were identified by means of automated database searching using Mascot (Matrix Science, London, UK) against Uni-Prot/Swiss-Prot.

3 Results and discussion

3.1 Overall metabolomic profile and amino acids

We analyzed metabolomic profiles of normal and tumor tissues obtained from nine lung and seven prostate cancer patients by using CE-TOFMS. Based on their *m/z* values and migration times, 114 and 86 metabolites were measured in the lung and prostate tissues, respectively (Supplementary Table S1), and visualized on a metabolome-wide pathway map (Supplementary Fig. S1) using VANTED software (Junker et al. 2006). The metabolomic data were then normalized and hierarchically clustered on both the metabolite and sample axes for a heat map representation (Supplementary Fig. S2) and further analyzed by principal component analysis (PCA) using MeV software (Saeed et al. 2003). Thirty-nine metabolites including glycolytic and TCA cycle intermediates, amino acids, and purine nucleoside phosphates, were absolutely quantified (Supplementary Table S2). PCA indicated that tumor metabolomic profiles were much more heterogeneous than their normal counterparts and comprised multiple clusters (Fig. 1a). With reference to the patient information (Table 1) and the hierarchically-clustered samples (Supplementary Fig. S2), tumor types appeared to play a greater part than tumor stage or differentiation status in altering the overall metabolomic profile in lung cancer, whereas differentiation status contributed more in prostate cancer. Indeed, the cluster of squamous cell carcinoma (SCC) patients (L1–3 and L7) was well-distinguished from that of adenocarcinoma (L4, L6 and L9) and pleomorphic carcinoma (L5). This may reflect the intrinsic pathological difference that adenocarcinoma cells but not squamous carcinoma cells retain their function of secreting mucus as glandular epithelial cells. In prostate samples, poorly differentiated prostate tumors (P2–4) were distant from the cluster of moderately differentiated (P1 and P5–7) tumors, which overlapped with that of normal samples. This may be due to higher duct-forming capacity and hormone response of well-differentiated prostate tumors, as well as normal prostate cells, than that of poorly differentiated tumors.

Both lung and prostate tumor samples were well-separated primarily along the PC1 axis; thus, factor loadings for the PC1 axis were evaluated. Correlations with the PC1 were particularly high in branched-chain amino acids (BCAAs) such as Val ($R = -0.97$), Ile (−0.97), and Leu (−0.89) in lung, and Leu (−0.87) in prostate samples (Supplementary Fig. S3). BCAAs are known to be avidly taken up by tumors and highly oxidized in cancer patients (Baracos and Mackenzie 2006), and thus may serve as effective indicators for diagnosing lung tumors. In fact, average lung tumor concentrations of all the 19 amino acids measured were higher than their respective normal levels, as were average prostate tumor levels of all the amino acids except Asp, Ile and Met (Fig. 1b). This is possibly due to hyperactivity of protein degradation and amino acid transporters in tumor cells (Fuchs and Bode 2005; Vander Heiden et al. 2009). Although average tumor levels of most amino acids in lung samples were significantly higher than their respective normal levels, normal and tumor Asp levels were comparable. Asp may be actively consumed as a precursor for nucleic acids and these TCA cycle intermediates, because tumor concentrations of malate, fumarate and succinate were significantly higher than the normal levels. In prostate tissues, levels of some amino acids such as Asn, Lys, Phe, Ser and Tyr and total essential amino acids were particularly higher in poorly differentiated tumors (P2–4; black in Fig. 1b) than moderately differentiated tumors (P1 and P5–7; gray in Fig. 1b), of which levels were comparable to the corresponding normal levels (Fig. 1b), implying enhancement of acquiring the amino acids upon dedifferentiation of prostate cancer cells.

3.2 Energy charge and adenosine and guanosine phosphates

Adenylate and guanylate energy charges (([RTP] + 0.5 × [RDP])/([RTP] + [RDP] + [RMP]), R = A or G) were lower in lung tumor than normal tissues (Fig. 2a); however, tumor levels were significantly higher than normal levels for ATP (3.8-fold), GTP (4.2-fold), and the other adenosine and guanosine phosphates (1.9–7.9-fold), and hence total adenylates (4.5-fold) and guanylates (4.0-fold). Tumor concentrations of these metabolites were relatively higher in all the SCC samples (L1–3 and L7; black in Fig. 2a) than the others (gray in Fig. 2a) such as L5 and L6, whose overall tumor metabolomic profiles resembled their respective normal profiles (Fig. 1). Purine synthesis may thus be hyperactivated in lung tumors, especially SCC, probably with a high basal ATP ↔ ADP turnover and purine salvage for maximizing their growth. Although prostate tissues showed much less normal-versus-tumor

differences, tumor ADP level was significantly lower than normal level (Fig. 2b). High absolute concentrations of ADP and GDP among other purine nucleoside phosphates are unique to prostate tissues, and ATP and AMP levels were relatively higher in poorly differentiated tumors (P2–4; black in Fig. 2b) than moderately differentiated tumors (P1 and P5–7; gray in Fig. 2b). This might be due to a differential expression of adenylate kinase catalyzing the reaction, 2ADP ↔ ATP + AMP, which is undetectable in adult prostate but shows activity along with its malignant alteration (Hall et al. 1985).

3.3 Glycolytic and TCA cycle intermediates and phosphorylated enzymes

Most glycolytic and TCA cycle intermediates were absolutely quantified (Fig. 3a), and phosphorylation levels of associated enzymes were also examined (Fig. 3b). Tumor lactate levels were higher than normal levels in both lung and prostate tissues, indicating their enhanced glycolysis and lactate fermentation, which reaffirmed the Warburg effect in cancer. Lung tumor levels of fructose 6-phosphate and fructose 1,6-bisphosphate were significantly lower and higher, respectively, than their corresponding normal levels. This may be partly explained by significantly high tumor levels of S386 phosphorylation in phosphofructokinase, which enhances its activity (Brand and Soling 1975), and thus the overall glycolytic flux because it is a bottleneck enzyme. Although tumor levels of S83 phosphorylation in glyceraldehyde 3-phosphate dehydrogenase and S203 in phosphoglycerate kinase-1 were significantly higher than their respective normal levels, their functional impacts are unknown. Tumor level of S37 phosphorylation of pyruvate kinase, which enhances its activity (Le Mellay et al. 2002), was significantly higher than the normal level. This may rationalize the trend that phosphoenolpyruvate and pyruvate were significantly lower and higher, respectively, in tumor than normal tissues. Tumor levels of S293 and S291 phosphorylation in pyruvate dehydrogenase, which inhibit its activity (Korotchkina and Patel 2001; Patel and Korotchkina 2001), were significantly higher than normal levels in all the lung cancer patients, except L6. This inhibition may contribute to the enhanced glycolysis and resulting lactate accumulation in lung tumors. In prostate tissues, however, most glycolytic intermediates were not detected, probably owing to inevitable overdilution of the samples for reducing polyamine concentrations, which otherwise adversely interfere with CE-TOFMS analysis. Trivial differences were observed between normal and tumor prostate phosphorylation levels of most glycolytic enzymes except glucose 6-phosphate isomerase (G6PI); nevertheless, the impact of elevated phosphorylation on the activity of G6PI is uncertain. Although intriguing, there was no apparent correlation between significantly high tumor levels of S481 phosphorylation in ATP citrate lyase in SCC samples, L1, L3

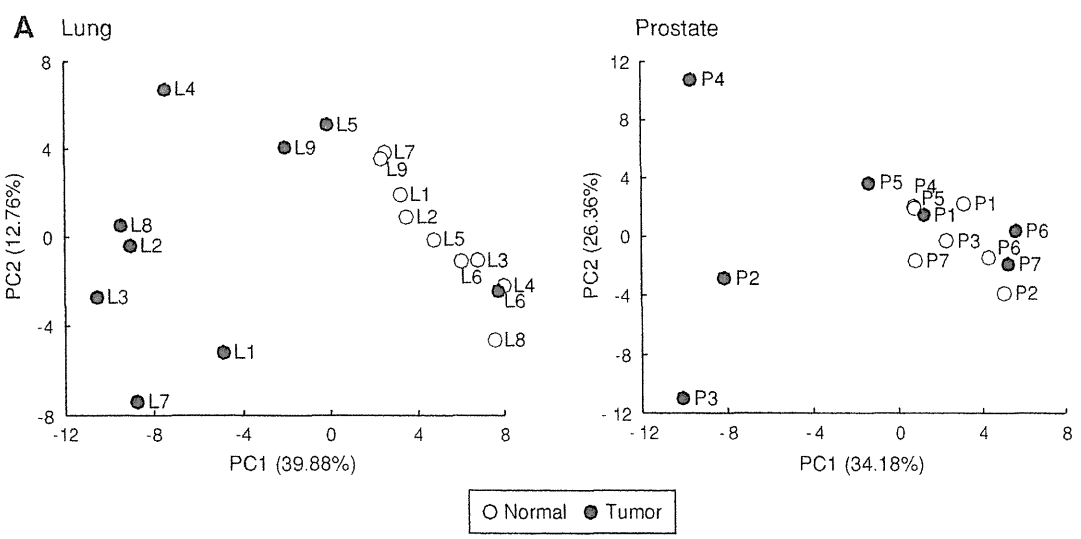

Fig. 1 **a** Score plots of PCA using the normalized metabolomic data of paired normal and tumor tissues obtained from lung (*left*) and prostate (*right*) cancer patients. The sample codes correspond to the patient IDs listed in Table 1. *Percentage values* indicated on the axes represent the contribution rate of the first (PC1) and the second (PC2) principal components. **b** Quantified levels of amino acids in normal (*left, open dots*) and tumor (*right, filled dots*) tissues obtained from lung and prostate cancer patients. *Horizontal bars* represent mean ± SD of normal (*left*) and tumor (*right*) samples and each connected pair represents the values for the same patient. *Gray dots* represent the values for patients with non-SCC lung cancer (L4–L6, L8 and L9) and patients with moderately differentiated prostate cancer (P1 and P5–7). *N.D.* indicates that the metabolite level was below the detection limit of the analysis. *Asterisks* indicate the significant differences between normal and tumor tissue levels based on the Wilcoxon signed-rank test (*$p < 0.05$; **$p < 0.01$; and ***$p < 0.001$)

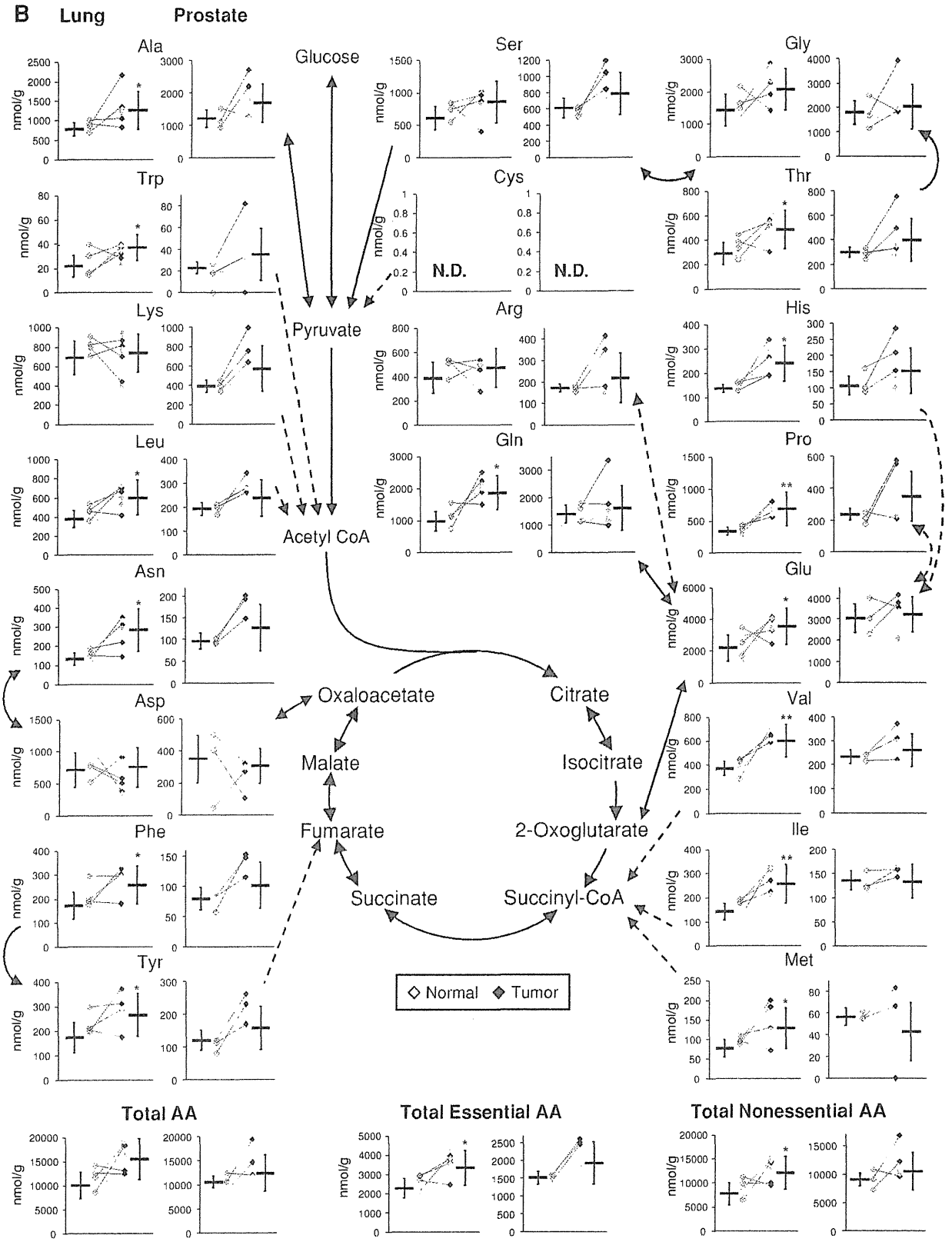

Fig. 1 continued

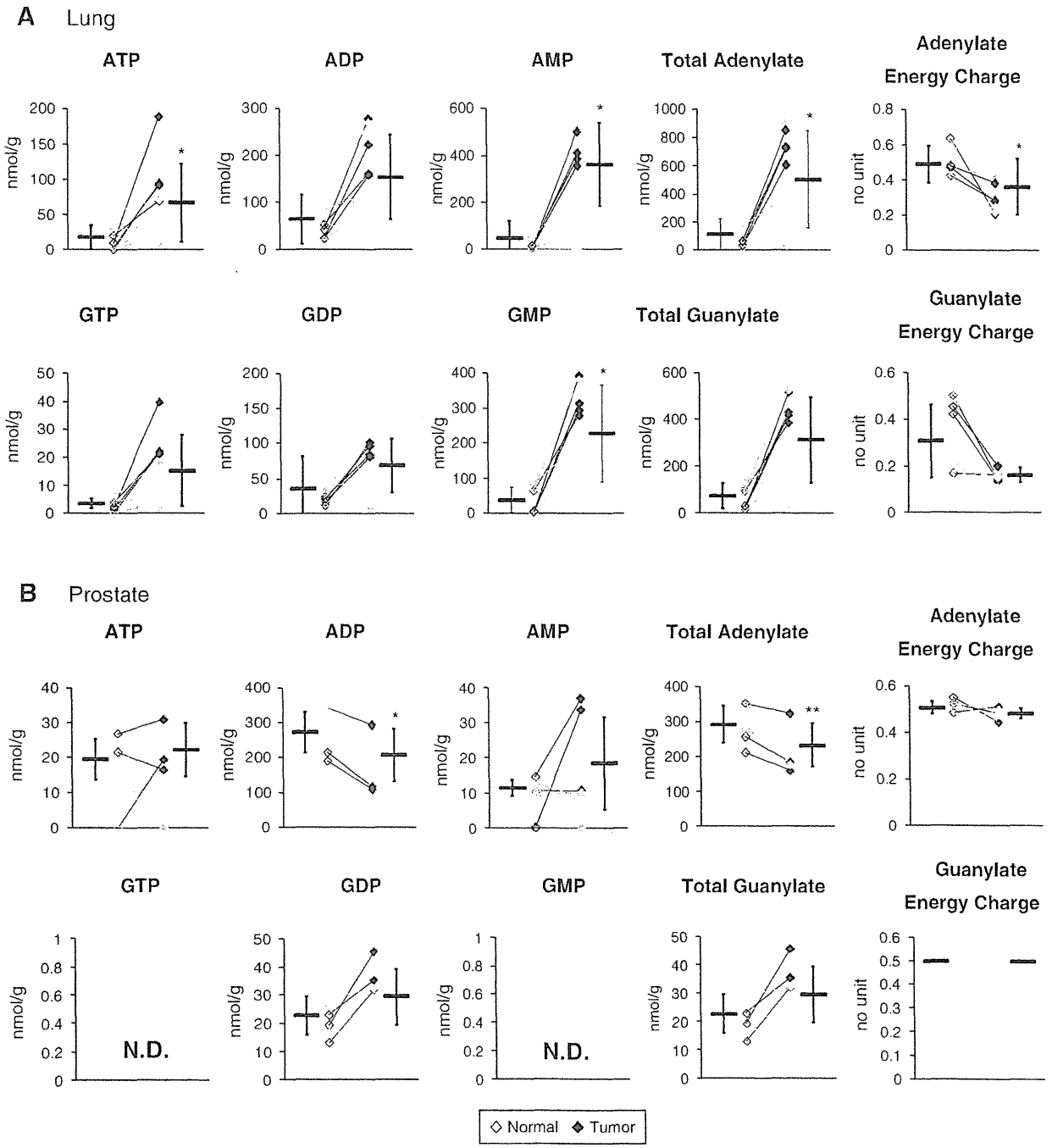

Fig. 2 Adenosine and guanosine phosphates, total adenylates and guanylates, and adenylate and guanylate energy charges of normal (*left, open dots*) and tumor (*right, filled dots*) tissues obtained from lung (**a**) and prostate (**b**) cancer patients. *Horizontal bars* represent mean ± SD of normal (*left*) and tumor (*right*) samples and each connected pair represents the values for the same patient. *Gray dots* represent the values for patients with non-SCC lung cancer (L4–L6, L8 and L9) and patients with moderately differentiated prostate cancer (P1 and P5–7). *N.D.* indicates that the metabolite level was below the detection limit of the analysis. *Asterisks* indicate the significant differences between normal and tumor tissue levels based on the Wilcoxon signed-rank test (*$p < 0.05$; **$p < 0.01$; and ***$p < 0.001$)

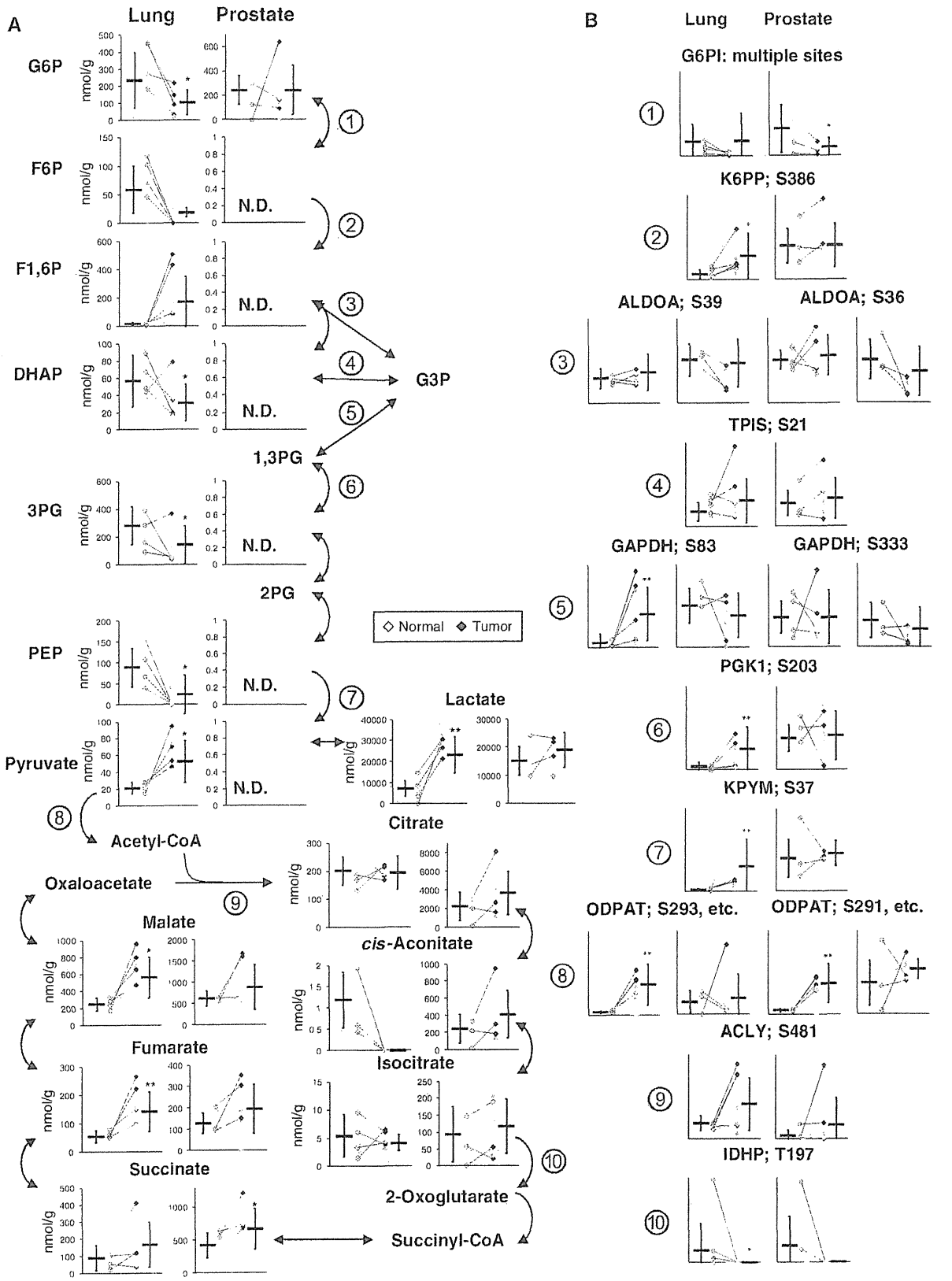
A
Lung
Prostate
G6P
F6P
F1,6P
DHAP
G3P
1,3PG
3PG
2PG
PEP
Pyruvate
N.D.
nmol/g
◇ Normal ◆ Tumor
Lactate
Citrate
Acetyl-CoA
Oxaloacetate
Malate
Fumarate
Succinate
cis-Aconitate
Isocitrate
2-Oxoglutarate
Succinyl-CoA
B
Lung
Prostate
G6PI: multiple sites
K6PP; S386
ALDOA; S39
ALDOA; S36
TPIS; S21
GAPDH; S83
GAPDH; S333
PGK1; S203
KPYM; S37
ODPAT; S293, etc.
ODPAT; S291, etc.
ACLY; S481
IDHP; T197

◀ **Fig. 3** Quantified levels of glycolytic and TCA cycle intermediates (**a**) and phosphorylation levels of each phosphorylation site in associated enzymes (**b**) in normal (*left, open dots*) and tumor (*right, filled dots*) tissues obtained from lung and prostate cancer patients. *Encircled numbers* in (**a**) indicated next to the metabolic reactions involved in glycolysis and the TCA cycle correspond to the associated enzymes in (**b**). *Horizontal bars* represent mean ± SD of normal (*left*) and tumor (*right*) samples and each connected pair represents the values for the same patient. *Gray dots* represent the values for patients with non-SCC lung cancer (L4–L6, L8 and L9) and patients with moderately differentiated prostate cancer (P1 and P5–7). *N.D.* indicates that the metabolite level was below the detection limit of the analysis. *Asterisks* indicate the significant differences between normal and tumor tissue levels based on the Wilcoxon signed-rank test (*$p < 0.05$; **$p < 0.01$; and ***$p < 0.001$). *G6PI* glucose 6-phosphate isomerase; *K6PP* 6-phosphofructokinase; *ALDOA* aldolase A; *TPIS* triosephosphate isomerase; *GAPDH* glyceraldehydes 3-phosphate dehydrogenase; *PGKI* phosphoglycerate kinase 1; *KPYM* pyruvate kinase isozymes M1/M2; *ODPAT* pyruvate dehydrogenase E1 component subunit alpha; *ACLY* ATP-citrate synthase; and *IDHP* isocitrate dehydrogenase

and L7, and their citrate concentrations. The impact of elevated phosphorylation levels of T197 in isocitrate dehydrogenase in normal L2 and P2 samples was also unclear. We need a larger number of sample sets in order to validate these results and provide further insight into possible correlations between phosphorylated states of the enzymes and metabolomic profiles.

Levels of all the quantified TCA cycle intermediates were higher in tumor than normal prostate tissues (Fig. 3a), which may be related to the typically hypoxic microenvironment of prostate tissues, because most TCA cycle intermediates are known to increase under hypoxia, while their flux through the pathway remains low (Wiebe et al. 2008). Average prostate citrate concentrations were >11-fold higher than in lung. This was partly due to a high concentration of zinc in the prostate, which inhibits m-aconitase and results in citrate accumulation (Mycielska et al. 2009). Prostate tumor exhibits low zinc levels and elevated fatty acid synthesis consuming citrate, and thus its citrate level is typically lower than in normal tissues (Mycielska et al. 2009), which is, however, inconsistent with our results. Tumor citrate, *cis*-aconitate, and isocitrate levels in P1, P3 and P7 were consistently lower than their respective normal levels, leaving the possibility that zinc and m-aconitase activity levels may vary depending on a factor other than differentiation status.

Succinate, fumarate, and malate levels were markedly higher in both prostate and lung tumor tissues than their corresponding normal tissues (Fig. 3a), which was consistent with our previous results for colon and stomach tumor metabolomics (Hirayama et al. 2009). We recently obtained strong evidence that, especially under hypoxic and nutrient-deprived conditions, energy generation of cancer relies on fumarate respiration (Sakai et al. 2012; Tomitsuka et al. 2010). This confers upon cells the ability to produce ATP by harnessing fumarate to succinate conversion, rather than oxygen to water, as the final electron transport step via the reverse reaction of succinate dehydrogenase (Kita and Takamiya 2002). Accumulation of these metabolites in tumors may therefore be attributed to hyperactivity of fumarate respiration.

3.4 Tumor-specificity and organ-dependency in metabolic profiles

The metabolome data obtained from both lung and prostate tissues were collectively normalized and hierarchically clustered (Supplementary Fig. S4A). As a result, lung-versus-prostate differences in terms of the overall metabolomic profiles appeared to be more significant than normal-versus-tumor differences within the same organ, as observed in our previous comparative metabolome analyses in colon and stomach tissues (Hirayama et al. 2009). As expected, PCA with the collectively normalized data showed clear inter-organ differences along with the PC2 axis; however, the normal-versus-tumor distinctions were also observed along with the PC1 axis (Supplementary Fig. S4B). This suggests that, in the carcinogenic process, cells alter their metabolism with a certain 'metabolic directionality' that is independent of organ types while retaining much of the metabolism that is unique to their organs of origin. Metabolites that showed high correlations with the PC2 included several nucleosides, TCA cycle intermediates, and polyamines, which characterize the inter-organ metabolic differences (Supplementary Table S3). In contrast, most glucogenic amino acids such as Thr, Ile, Asn, Pro, His, Gln, and Ser were closely associated with the PC1 (Supplementary Table S3), suggesting that a hyper-production and/or -acquisition of a certain set of amino acids likely occurs in the course of tumorigenesis.

4 Conclusion

Overall tumor metabolomic profiles were found to be significantly different depending on tumor type in lung cancer and differentiation status in prostate cancer. Elevated tumor concentrations of almost all the amino acids, especially BCAAs, were identified in an organ-independent manner, and this trend was more prominent in SCC than the other tumor types in lung cancer and in poorly rather than moderately differentiated prostate cancer. Analyses with much more samples, however, are necessary in order to statistically confirm these unique subtype-specific metabolic fingerprint of cancer. In contrast, through our combined metabolomic and phosphorylated enzyme analyses, we found that glycolytic and TCA cycle intermediates,

levels of which are probably associated with enzyme phosphorylation levels, exhibited significant organ dependency, reaffirming that inter-organ metabolomic differences are generally more significant than normal-versus-tumor differences within the same organ. Nonetheless, metabolomic profiles of both lung and prostate tumors appear to have a common 'directionality' along with their increasing malignancy represented by high concentrations of a certain set of glucogenic amino acids. Taken together, we identified organ-dependent, tumor-specific, and tumor-pathology-dependent metabolic features, which highlights the need for a combined metabolomics and phosphoproteomics analysis on a broader scale with a larger number of sample sets for improving specificity and effectiveness of personalized anticancer therapeutics.

Acknowledgments The authors thank Dr. Masahiro Sugimoto for developing MasterHands software. This work was supported in part by a grant for the Third Term Comprehensive 10-year Strategy for Cancer Control from the Ministry of Health, Labour and Welfare (H.E.) and a grant from the Global COE Program entitled, "Human Metabolomic Systems Biology" (K.K.). This work was also supported by KAKENHI (Grant-in-Aid for Scientific Research) on Priority Areas "Systems Genomes" and on "Lifesurveyor" from the Ministry of Education, Culture, Sports, Science and Technology (MEXT) of Japan as well as research funds from the Yamagata prefectural government and the City of Tsuruoka (Y.O., M.T., and T.S.).

References

Baracos, V. E., & Mackenzie, M. L. (2006). Investigations of branched-chain amino acids and their metabolites in animal models of cancer. *Journal of Nutrition, 136*, 237S–242S.

Brand, I. A., & Soling, H. D. (1975). Activation and inactivation of rat liver phosphofructokinase by phosphorylation—dephosphorylation. *FEBS Letters, 57*, 163–168.

Fuchs, B. C., & Bode, B. P. (2005). Amino acid transporters ASCT2 and LAT1 in cancer: Partners in crime? *Seminars in Cancer Biology, 15*, 254–266.

Hall, M., Mickey, D. D., Wenger, A. S., & Silverman, L. M. (1985). Adenylate kinase: An oncodevelopmental marker in an animal model for human prostatic cancer. *Clinical Chemistry, 31*, 1689–1691.

Heiden, M. G. V., Cantley, L. C., & Thompson, C. B. (2009). Understanding the Warburg effect: The metabolic requirements of cell proliferation. *Science, 324*, 1029–1033.

Hirayama, A., Kami, K., Sugimoto, M., Sugawara, M., Toki, N., Onozuka, H., et al. (2009). Quantitative metabolome profiling of colon and stomach cancer microenvironment by capillary electrophoresis time-of-flight mass spectrometry. *Cancer Research, 69*, 4918–4925.

Ishihama, Y. (2005). Proteomic LC-MS systems using nanoscale liquid chromatography with tandem mass spectrometry. *Journal of Chromatography A, 1067*, 73–83.

Ishihama, Y., Rappsilber, J., Andersen, J. S., & Mann, M. (2002). Microcolumns with self-assembled particle frits for proteomics. *Journal of Chromatography A, 979*, 233–239.

Junker, B. H., Klukas, C., & Schreiber, F. (2006). VANTED: A system for advanced data analysis and visualization in the context of biological networks. *BMC Bioinformatics, 7*, 109.

Kita, K., & Takamiya, S. (2002). Electron-transfer complexes in *Ascaris* mitochondria. *Advances in Parasitology, 51*, 95–131.

Korotchkina, L. G., & Patel, M. S. (2001). Site specificity of four pyruvate dehydrogenase kinase isoenzymes toward the three phosphorylation sites of human pyruvate dehydrogenase. *Journal of Biological Chemistry, 276*, 37223–37229.

Kyono, Y., Sugiyama, N., Imami, K., Tomita, M., & Ishihama, Y. (2008). Successive and selective release of phosphorylated peptides captured by hydroxy acid-modified metal oxide chromatography. *Journal of Proteome Research, 7*, 4585–4593.

Le Mellay, V., Houben, R., Troppmair, J., Hagemann, C., Mazurek, S., Frey, U., et al. (2002). Regulation of glycolysis by Raf protein serine/threonine kinases. *Advances in Enzyme Regulation, 42*, 317–332.

Mycielska, M. E., Patel, A., Rizaner, N., Mazurek, M. P., Keun, H., Ganapathy, V., et al. (2009). Citrate transport and metabolism in mammalian cells: Prostate epithelial cells and prostate cancer. *BioEssays, 31*, 10–20.

Ohashi, Y., Hirayama, A., Ishikawa, T., Nakamura, S., Shimizu, K., Ueno, Y., et al. (2008). Depiction of metabolome changes in histidine-starved *Escherichia coli* by CE-TOFMS. *Molecular BioSystems, 4*, 135–147.

Olsen, J. V., de Godoy, L. M., Li, G., Macek, B., Mortensen, P., Pesch, R., et al. (2005). Parts per million mass accuracy on an Orbitrap mass spectrometer via lock mass injection into a C-trap. *Molecular and Cellular Proteomics, 4*, 2010–2021.

Patel, M. S., & Korotchkina, L. G. (2001). Regulation of mammalian pyruvate dehydrogenase complex by phosphorylation: Complexity of multiple phosphorylation sites and kinases. *Experimental & Molecular Medicine, 33*, 191–197.

Rappsilber, J., Ishihama, Y., & Mann, M. (2003). Stop and go extraction tips for matrix-assisted laser desorption/ionization, nanoelectrospray, and LC/MS sample pretreatment in proteomics. *Analytical Chemistry, 75*, 663–670.

Rappsilber, J., Mann, M., & Ishihama, Y. (2007). Protocol for micro-purification, enrichment, pre-fractionation and storage of peptides for proteomics using StageTips. *Nature Protocols, 2*, 1896–1906.

Saeed, A. I., Sharov, V., White, J., Li, J., Liang, W., Bhagabati, N., et al. (2003). TM4: A free, open-source system for microarray data management and analysis. *BioTechniques, 34*, 374–378.

Sakai, C., Tomitsuka, E., Esumi, H., Harada, S., & Kita, K. (2012). Mitochondrial fumarate reductase as a target of chemotherapy: From parasites to cancer cells. *Biochimica et Biophysica Acta, 1820*, 643–651.

Sugiyama, N., Masuda, T., Shinoda, K., Nakamura, A., Tomita, M., & Ishihama, Y. (2007). Phosphopeptide enrichment by aliphatic hydroxy acid-modified metal oxide chromatography for nano-LC-MS/MS in proteomics applications. *Molecular and Cellular Proteomics, 6*, 1103–1109.

Tomitsuka, E., Kita, K., & Esumi, H. (2010). The NADH-fumarate reductase system, a novel mitochondrial energy metabolism, is a new target for anticancer therapy in tumor microenvironments. *Annals of the New York Academy of Sciences, 1201*, 44–49.

Warburg, O. (1956). On the origin of cancer cells. *Science, 123*, 309–314.

Wiebe, M. G., Rintala, E., Tamminen, A., Simolin, H., Salusjarvi, L., Toivari, M., et al. (2008). Central carbon metabolism of *Saccharomyces cerevisiae* in anaerobic, oxygen-limited and fully aerobic steady-state conditions and following a shift to anaerobic conditions. *FEMS Yeast Research, 8*, 140–154.